Structures 51 (2023) 1773–1794

Contents lists available at ScienceDirect

Structures

journal homepage: www.elsevier.com/locate/structures

Development of integrated semi-active adaptive vibration control system for bridges subjected to traffic loads

Hengameh Farahpour [a], Farzad Hejazi [b,*]

[a] Department of Civil Engineering, University Putra Malaysia, Selangor, Malaysia
[b] Faculty of Environment and Technology, The University of West England, Bristol, United Kingdom

ARTICLE INFO

Keywords:
Real-time control
Viscous fluid damper
Bridge structure
Structural dynamic loads
Semi-active control
Fuzzy control algorithm

ABSTRACT

Nowadays, the fluid viscous damper is the most conventional energy dissipation system implemented in bridge structures to control the vibrations due to traffic loads. However, to effectively protect the bridge against frequent and severer vibrations, it is required to adapt the function of the damper according to the variable traffic loads. In this research, an Integrated Semi-Active Adaptive Vibration Control System is developed for the bridge structures. This control system consists of a Semi-Active Bypass Fluid Damper (SABFD), a programmable logic controller (PLC), pressure transducers, and displacement sensors. Semi-Active Bypass Fluid Damper is a hydraulic cylinder with a pair of external bypass pipes with motorized electric flow control valves which are installed in the middle of pipes to control the flow rate of the fluid. A programmable logic controller (PLC) is implemented to manage the operation of motorized valves according to the movement of the bridge.

Therefore, the integrated control system is able to function as a real-time controller during its operation. To develop the control system, the performance of the SABFD device has been assessed through analytical model of the various control valve positions. Then, according to the structure response, a fuzzy control algorithm has been adapted in the PLC controller.

Afterward, the prototypes of the SABFD and the PLC controller have been fabricated and a series of cyclic load tests have been conducted by using a dynamic actuator. The outcomes of the numerical analysis and results of the experimental tests revealed that the developed device is capable of generating a wide range of forces during device operation. The developed fuzzy control algorithm is then implemented to the finite element model of the bridge equipped with SABFD, and the results proved that the real-time control system effectively limits the bridge displacements according to the pre-defined fuzzy control rules.

1. Introduction

The majority of bridge failures occur due to underestimating deck displacements due to significant dynamic forces applied to the structural members over the operation life of the bridge. According to conclusive research works, bridge structures are often subjected to higher-than-expected dynamic loads, as a result of traffic, which reduces the service life of these critical structures [31].

In 2020, the impacts of traffic congestion on European road bridges have been studied and the loads model due to vehicle traffic was verified [13]. Also, the computed necessary safety margins showed the most frequently used load model is unable to demonstrate the real effect of the changing traffic loads on the bridges.

A series of full-scale tests and numerical calculations have been conducted to investigate the critical details of the operational life on twin 170 m long steel railway bridges [6]. At the same time, a new model of steel bridges under traffic loading was proposed by Yang Yu. To develop this model, a stress time history was utilized and transformed to cycle history to predict the crack growth of steel bridges in the time domain [33].

Dynamic responses of a highway bridge are numerically analyzed by employing the refined finite element (FE) models of a heavy truck and a simply-supported prototype highway bridge. A series of numerical simulations have been conducted to examine the heavy truck collision process on a typical four-span reinforced concrete (RC) bridge with two-pier bents [8].

A novel tuned mass damper (SAEC-PTMD) which can retune its frequency and damping ratio in real-time, is developed by Wang in 2020

* Corresponding author.
E-mail address: farzad.hejazi@uwe.ac.uk (F. Hejazi).

https://doi.org/10.1016/j.istruc.2023.03.107
Received 20 January 2023; Received in revised form 18 March 2023; Accepted 20 March 2023

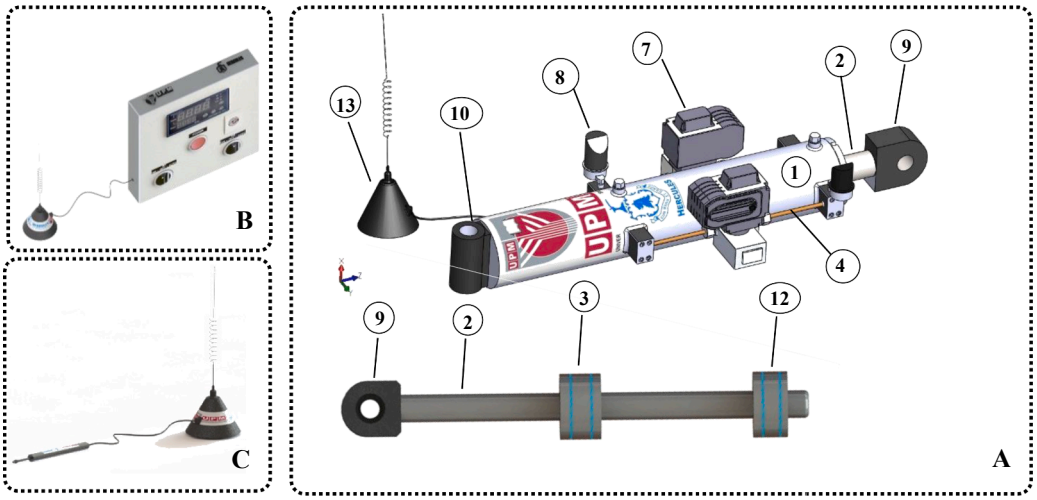

(a) Assembled view

No.	Component
A	Bypass Fluid Damper device
1	Hydraulic Cylinder
2	Piston Shaft
3	Piston Head
4	Bypass Pipes
5	Left Chamber of the Hydraulic Cylinder
6	Right Chamber of the Hydraulic Cylinder
7	Controllable Digital Motorized Ball Valves
8	Digital Pressure Transducer
9	Piston Shaft Connector
10	Hydraulic Cylinder Connector
11	Empty Seal Space
12	Shaft End-Head
13	Antenna for wireless communication system
B	Programmable logic controller (PLC)
C	LVDT Sensors and meter panel

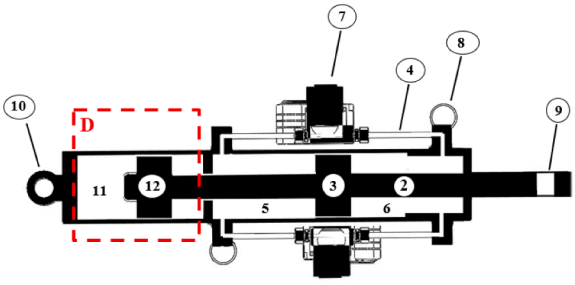

(b) Schematic section diagram

Fig. 1. Integrated Semi-Active system.

[27] and results shows that the new device functions more effective than an optimized passive TMD.

However, despite all the complications of bridge vibration and the numerous parameters incorporate regulations and standards in many countries, the natural frequencies and corresponding modes of vibration, the dynamic coefficient (a dynamic increase of stress or deformation), and the damping are the basic bridge vibration characteristics, which can be verified by experimental tests and monitoring.Benčat and Kohár [5].

A semi-active independent variable mass TMD (SAIVM-TMD) has been compared with other controllers implemented in a bridge subjected to crowd-induced stochastic excitation. The results prove the advantages of the new device according to the ability of adapt to the structural vibrational frequency changes [22].

A slender steel pedestrian bridge subjected to the vertical and lateral dynamic vibrations due to walking and wind loads has been strengthened by using a two-dimensional air spring based STMD (TDAS-STMD). The performance of the device has been evaluated in compare with a group of two optimized passive TMDs which implemented in vertical and lateral directions [28].

The flow inside the fluid damper was modeled by the Carreau-Yasuda (CY) and Phan-Thien & Tanner (PTT) constitutive equations. Elastic effects are quantified by applying a decomposition of the damper force into elastic and viscous components. It is thus concluded that theoretical approaches that rely on the assumption of one-dimensional flow in the piston-cylinder gap are of limited accuracy, even if they account for fluid viscoelasticity. [18].

The viscous damping coefficients of three fluids, water, edible oil, and gasoline engine oil were determined in terms of the inverse Mittag-Leffler function. The influence of the viscosity of the fluid was analyzed theoretically and experimentally in the spring-mass–viscodamper system. [7].

According to the increasing need to design safer bridges, active and semi-active control systems were developed as effective practical methods for vibration control. These systems are mostly defined by regulating stiffness and damping characteristics of the supplementary restrainer devices as well as changing the characteristics of the structure [17,11].

Semi-active control systems are a class of active control systems and derives from a passive control mechanism and dissipates energy on original concepts such as metal phase transition, viscoelastic material elongation, or fluid and sliding friction. In the semi-active control method, structural stability is provided, in the sense that semi-active systems use the structure's motion energy to create the control forces. A semi-active device will never destabilize a structural system whereas it can be destabilized by an active device [32].

A semi-active tuned mass damper (STMD) with variable stiffness and damping with a combined control algorithm is applied to an eight-story linear base-isolated structure and also a nonlinear one. Generally, STMD has the best control effect in both linear and nonlinear models and can mitigate the structural first-mode response effectively [23].

A non-dominated sorting genetic algorithm was used as a multi-objective optimal design of semi-active fluid viscous dampers [4]. The designed optical system included the maximum damping coefficient and

control algorithm parameters as design variables and significantly reduced the seismic response of the structure.

In order to overcome detuning shortcoming of a passive MTMD system, an adaptive-passive variable mass multiple TMD (APVM-MTMD) system is proposed by Wang in 2020. This device can automatically retune itself by varying its mass and has the best vibration control effect compared to the mistuned MTMD system case [25].

An adaptive-passive eddy current pendulum TMD (APEC-PTMD) is also presented with the ability of retune the frequency through varying the pendulum length, and retune the damping ratio through adjusting the air gap between permanent magnets and conductive plates [21]. The device is applied to a benchmark 40-story tall building including SSI and four different soil conditions subjected to the 44 far-field earthquake excitations. The study proves excellent control effect of the device compared to the without TMD case at the same time [26].

Numerical simulations show that semi-active control can reach active control performance if the design goal is to reduce bearing response. A semi-active method for mitigation of random and harmonic forced vibrations of frame structures has been proposed and tested [16]. This method stimulates the transfer of vibration energy from low-order into high-order natural modes of vibration. The effectiveness of the approach was confirmed numerically and experimentally.

Adaptive semi-active vibration control with an internal model of the time-varying moving load was studied. The asymptotic stability of the closed-loop system and performance improved and compared to passive and optimal open-loop strategies [29].

A hybrid control method that adapts a hierarchical structure consisting of several sub-controllers and a fuzzy supervisor is introduced by Park [15]. For a comparison of the seismic performance, an optimally designed LQG system was also simulated for the benchmark bridge.

To control the wind vibration, an adaptive-passive variable pendulum TMD (APVP-TMD) is developed and its effectiveness is verified through both discrete and continuous models and comparison with experiment outputs. The results demonstrate that the APVP-TMD can identify the optimal frequency and retune itself effectively [24].

Hence, the fuzzy control algorithm was proven a proper control strategy for the semi-active control system [34].

Thus, the main aim of this study is to develop an Integrated Semi-Active Adaptive Vibration Control System consisting of a new Semi-active Bypass Fluid Damper (SABFD), a PLC controller, and sensors to measure bridge displacement and viscous oil pressure (in viscous damper) during the operation. The new SABFD is a viscous damper that utilized two bypass pipes from both sides with a motorized control valve installed in each bypass pipe to control the oil flow within the cylinder. The PLC controller receives the bridge movement data from the displacements sensors and computes the required valve position for the SABFD device. The calculated valve position is sent from the PLC controller as a command to the motorized valves which are installed in the middle of bypass pipes of the SABFD device. The real-time control of the valve position results in the real-time pressure control inside the damper and changes the overall performance of the SABFD device. Then, the developed control system is implemented for real-time control of a bridge according to the pre-defined fuzzy control algorithms in the PLC system.

2. Development of Integrated Adaptive Vibration Control System

The proposed Integrated Adaptive Vibration Control System as shown in Fig. 1, is developed by utilizing a new Semi-Active Bypass Fluid Damper device (Part A), a programmable logic controller (Part B), and bridge movement measurement instruments (Part C). Details regarding of development of each part are demonstrated in the following subsections:

2.1. Development of Semi-Active Bypass Fluid Damper device (SABFD)

In this research, a new adjustable Semi-Active Bypass Fluid Damper device (Part A in Fig. 1) is developed to adapt its function according to the required performance. For this purpose, a steel hydraulic cylinder with inlet and outlet ports (label 1) and a steel piston shaft (label 2) with a piston head (label 3) are implemented. A pair of external bypass pipes (label 4) are utilized on both sides of the cylinder to flow the viscous fluid or oil from one chamber of the cylinder (label 5) to another side during the movement of the piston (label 6). Two controllable digital motorized ball valves (label 7) are positioned in the middle of the bypass pipes to adjust the flow pressure rate of the hydraulic oil throughout the bypass pipe during the movement of the piston and control performance of the fluid damper.

These digital motorized ball valves (label 7) are able to change the oil flow inside the bypass pipe by receiving signals from the PLC controller (label B). Communication between motorized digital ball valves and A programmable logic controller (Label B) can be conducted through cables or wireless communication systems. For this purpose, an antenna (Label 13) has been connected to the fluid damper device as a part of the wireless communication system. Therefore, the digital motorized ball valves are connected and synchronized with the PLC controller (label B) through a cable or wireless real-time data transferring system to send and receive data related to the required position of the valve during the operation of the device. The ball valve position can change between zero to 90 degrees to control the fluid flow between two chambers through bypass pipes during the movement of the shaft and piston.

Two digital pressure transducers (label 8) are also installed in bypass pipes to acquire and monitor oil pressure in the bypass pipe during the operation of the device. The real-time measured data for oil pressure is also sent to the PLC controller through a cable or wireless real-time data transferring system to use by a developed controller algorithm to determine the required changes in flow pressure by controllable digital motorized ball valves.

A pined hinge is welded to the end of the piston shaft (label 2) as a piston shaft connector (label 9) and also another pinned hinge is welded to another end part of the cylinder (label 1) as a hydraulic cylinder connector (label 10).

Then the SABFD device is installed in the bridge and connected to the deck and pier of the bridge through the piston shaft connector (label 9) and hydraulic cylinder connector (label 10). Part D as shown in the section view in Fig. 1 (b), includes an empty sealed space inside the hydraulic cylinder (Label 11) and the end head of the shaft (Label 12). The empty space gap is set inside the hydraulic cylinder (Label 11) to make enough space for the shaft (Label 2) and shaft end-head (Label 12) to move during the operation of the device.

Then, through this configuration, the viscous fluid damper functions as a double shaft damper with symmetric force–displacement performance, and the generated force during pulling and pushing action are equal. Also, the end head aligns the shaft movement which leads to avoiding any inclination of the shaft when the device is subjected to any unexpected buckling.

2.2. Development of a programmable logic controller (Part B)

A special programmable logic controller (PLC) has been developed in this research study to conduct real-time control of fluid damper performance by changing the oil flow throughout the bypass pipe using Digital Motorized Ball Valves.

Since the resultant force of the fluid damper changes by varying the fluid flow rate inside the bypass pipes, therefore PLC system controls the damping force of the device by changing valve positions to adjust oil pressure according to the defined control algorithm.

For this purpose, a fuzzy logic algorithm has been developed and coded in the PLC system to perform real-time control of the valve position and also optimize the performance of the fluid damper based on

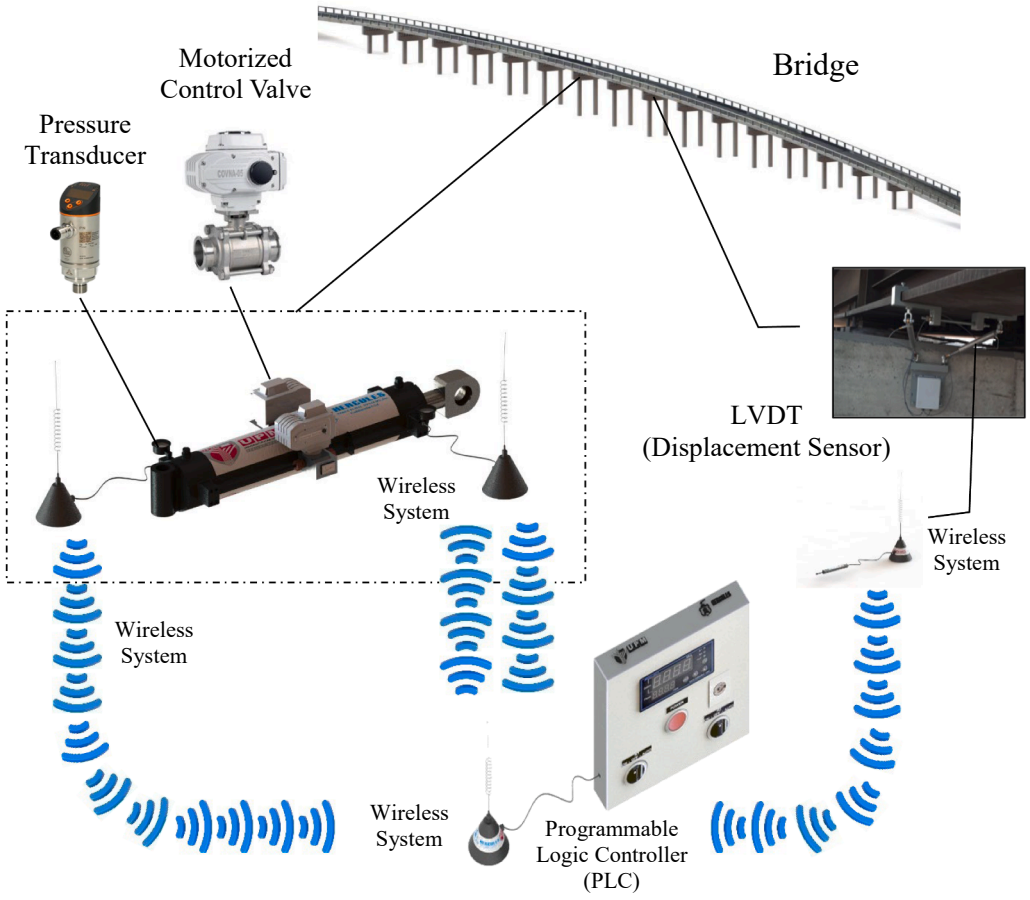

Fig. 2. Integrating the Components of Adaptive Vibration Control System.

the movement of the bridge due to applied traffic load. Thereby, a set of Linear Variable Differential Transformer (LVDT) sensors (Label C) is installed on the bridge deck to measure the displacement of the bridge during its operation. The LVDT sensors measure the bridge deck displacement and transfer the data to the LVDT panel meter.

The panel meter reads the signals from sensors, converts the signals, and transmits the readable signals to the PLC controller through a cable or wireless communication system.

So, the PLC controller (Label B) received displacement data from linear variable differential transformer (LVDT) displacement sensors (Label C) through the LVDT panel meter and compute the required valve position according to the internal fuzzy control algorithm to minimize bridge movement and then send the position command to the ball valves to adjust oil flow using Controllable Digital Motorized Ball Valves (Label 7).

As mentioned before, the ball valve is able to rotate between 0° to 90° positions. Therefore, in this study, the β parameter has been defined to specify the action of the digital motorized ball valve based on valve position. Then, β is defined as 0% for the valves in the position of 0° which valves are totally open, therefore the minimum damping performance is assigned to the fully open valve position. So, $\beta = 0$ demonstrates a fully open valves condition and the minimum damping characteristics of the SABFD damper device. Whereas, β is defined as 100% for valves in 90° position when the valves are fully closed and the device exhibits its maximum restraining response to limit the structure movements.

Variations of β change the damping coefficient, and stiffness of the SABFD damper. This newly defined parameter, change the resultant force and the function of the SABFD device by controlling oil flow. This procedure is followed by sending valve feedback data to the PLC controller.

So, after receiving the displacement data, the PLC controller computes the required valve parameter (β) according to the internal Fuzzy control algorithm and sends the command of β value to the Digital Motorized Ball Valve to take action accordingly.

The real-time communication between PLC (Label B), digital pressure transducers (Label 8) on the bypass pipe in the SABFD device, and also LVDT (Label C) on the bridge deck is performing continuously to exchange displacement, valve position, and required β data throughout the operation of the system.

2.3. *Integrating the components of adaptive vibration control system*

As shown in Fig. 2, all developed components for adaptive vibration control systems are integrated and synchronized together to conduct real-time control of bridge movement using a fluid damper device according to the displacement of the bridge deck.

Through this mechanism, the installed LVDTs (Label C) on the bridge are measuring the displacement of the bridge deck under applied traffic load and these data from various LVDTs are collected by the displacement meter panel (Label C). Then displacements data are immediately transferred to the Programmable Logic Controller (Label B) via a wireless communication system. Both LVDT meter panel and PLC controller are utilized with an antenna or cable (Label 13) for the communication system.

At the same time, the data regarding the position of the valve in Controllable Digital Motorized Ball Valves (Label 7) and also fluid pressure bypass pipe (Label 4) measured by the Digital Pressure Transducer (Label 8) are sent to the PLC (Label B) through the communication system. Similarly, Antennas or cables (Label 13) are installed in both

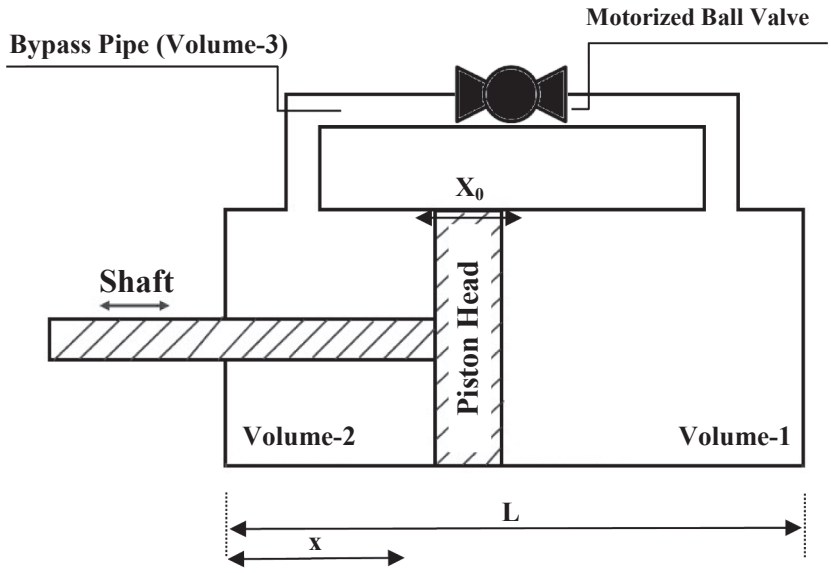

Fig. 3. The simplified diagram of the SABFD device.

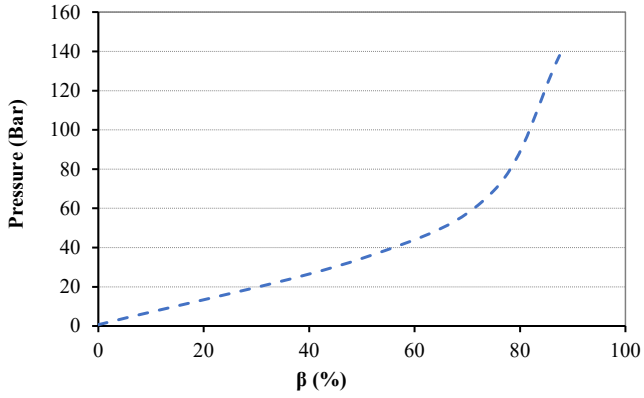

Fig. 4. Fluid pressure in the bypass pipes according to β.

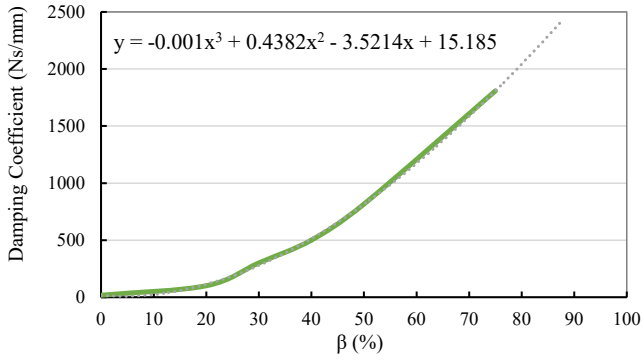

Fig. 5. Numerically predicted damping coefficient of the SABFD device.

Controllable Digital Motorized Ball Valves (Label 7) and Digital Pressure Transducers (Label 8) for the communication systems.

Thereafter, based on received data regarding bridge displacement, valve position, and fluid pressure, the developed fuzzy control algorithm in the PLC determines the most suitable valve condition to be applied by the Controllable Digital Motorized Ball Valves (Label 7) in order to obtain the best performance of Bypass Fluid Damper device (A) to minimize bridge movement. Then, the new determined valve position is sent from PLC (Label B) to the Controllable Digital Motorized Ball Valves (Label 7) as an immediate command to apply through the communication system. Afterward, the valve adjusts the fluid flow and pressure in the bypass pipe (Label 4), and consequently, the piston (Labels 2 and 3) moves inside the cylinder (Label 1) to generate desirable damper force to minimize bridge movement. This process is continuedly repeated during the time of bridge operation to diminish the vibration of the bridge through the adaptive vibration control system.

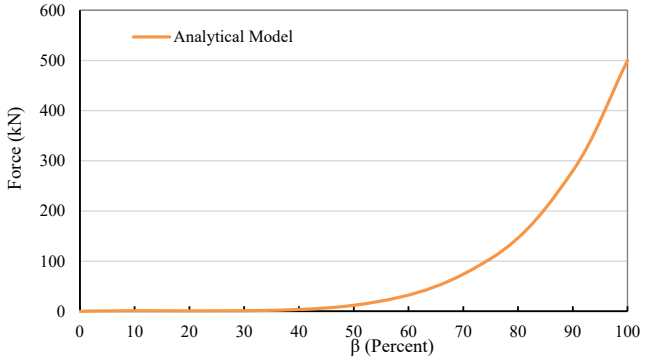

Fig. 6. The numerically predicted force of the SABFD device.

So, as demonstrated, all the components are integrated and synchronized to communicate and transfer the data between each other to perform real-time control mechanism using Bypass Fluid Damper for the bridge structure based on its various vibration due to traffic load or any external excitations.

3. Development of the analytical model

To develop the analytical model of the SABFD device, a simplified diagram of the damper has been designed as shown in Fig. 3. The force and action of the damper and also the pressure on the left/right chamber of the piston are assumed to be equal for the movement of the piston head in both directions. Also, friction between the piston and the cylinder is considered to be negligible.

As shown in Fig. 3, when the piston moves from its equilibrium point to the right direction, the pressure in volume-1 rises due to compression,

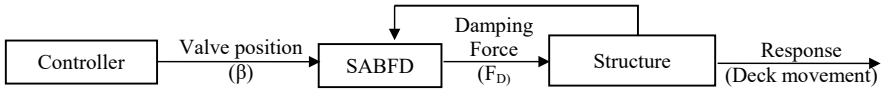

(a) Open-loop control diagram

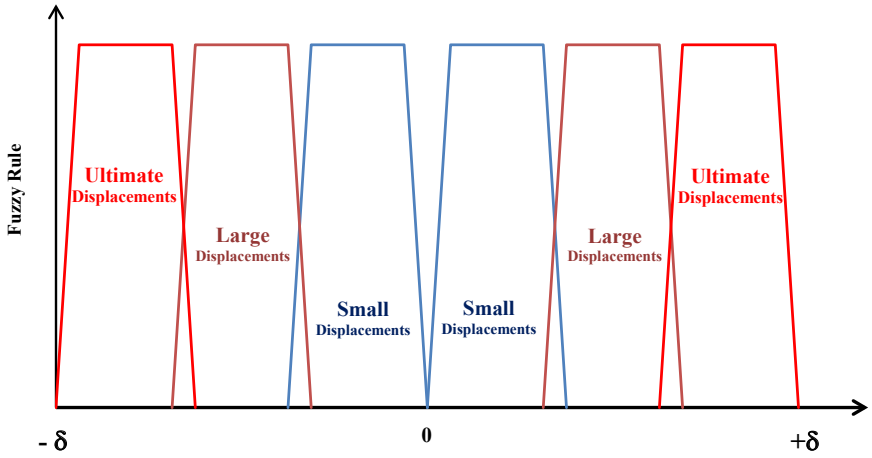

(b) Fuzzy control diagram in this study

Fig. 7. Open-loop fuzzy control configurations.

Table 1
Fuzzy logic parameters.

Function	β (%)	Fuzzy Rule (I)	Displacement (δ)
Safety Rule	0	Ultimate	$-17\ \text{mm} \geq \boldsymbol{\delta}$
Operation Rule	90	Large	$-17\ \text{mm} < \boldsymbol{\delta} \leq -7\text{mm}$
	50	Small	$-7\text{mm} < \boldsymbol{\delta} \leq 7\ \text{mm}$
	90	Large	$7\ \text{mm} < \boldsymbol{\delta} \leq 17\ \text{mm}$
Safety Rule	0	Ultimate	$\boldsymbol{\delta} > 17\ \text{mm}$

Fig. 8. Prototype of the SABFD control system.

while pressure in volume-2 decreases due to rarefaction. The fluid then starts to flow from volume-1 to volume-2 through the bypass pipe (volume-3). As long as the pressure in volume-1 is greater than the pressure in volume-2, the flow path stays the same.

When the piston head moves in the reverse direction, the pressure in volume-2 would be more than volume-1, and then the flow in the bypass pipe will flow reversely.

From the law of conservation of mass in volume-1 and 3, the exchange flow rate from the cylinder due to the piston movement can be given as [10] Equation (1).

$$\frac{dM_{32}}{dt} = A_{cl}\rho_1\frac{dX}{dt} - A_{cl}(L-X)\frac{d\rho_1}{dt} \tag{1}$$

where A_{cl} is cylinder cross-section area, ρ_1 is fluid density in volume-1 and $\frac{dM_{32}}{dt}$ is the mass flow rate through the bypass pipe. The parameters of L and X are highlighted in Fig. 3. According to the law of continuity of volume-2, Equation (2) can be written as:

$$\frac{dM_{32}}{dt} = A_{cl}\rho_2\frac{dX}{dt} + A_{cl}X\frac{d\rho_2}{dt} \tag{2}$$

where ρ_2 is fluid density in volume 2. The industrial oil that is used in the hydraulic system is considered to be incompressible. So, parameters ρ_1 and ρ_2 are identical and equal to ρ, and $\frac{d\rho_1}{dt} = \frac{d\rho_2}{dt} = 0$. With neglecting the effect of the boundary of the cylinder, the discharged mass flow from the cylinder can be written as follows:

$$\frac{dM_{32}}{dt} = A_{cl}\rho\frac{dX}{dt} \tag{3}$$

While the flow rate in the bypass pipe can be expressed as Equation (4).

$$\frac{dM_{32}}{dt} = v_{pp}\,\beta\,A_{pp}\,\rho \tag{4}$$

where v_{pp} is flow velocity inside the pipe and A_{pp} is the cross-section area of the pipe. Parameter β is denoted by the valve position in percentage. For example, β equal to 70% shows valves are 70 percent closed. The flow velocity inside the pipe is calculated from Equations (3) and (4) as follows:

$$v_{pp} = \frac{A_{cl}}{\beta A_{pp}}\frac{dX}{dt} \tag{5}$$

And from Bernoulli's Equation between volume-1 and volume-3, the pressure of fluid inside the bypass pipe is:

$$\frac{V_1^2}{2g} + \frac{p_1}{\rho g} + z_1 = \frac{V_3^2}{2g} + \frac{p_3}{\rho g} + z_3 + h_L \tag{6}$$

where v_1, v_3, and p_1, p_3 show fluid velocity and pressure inside volume-1

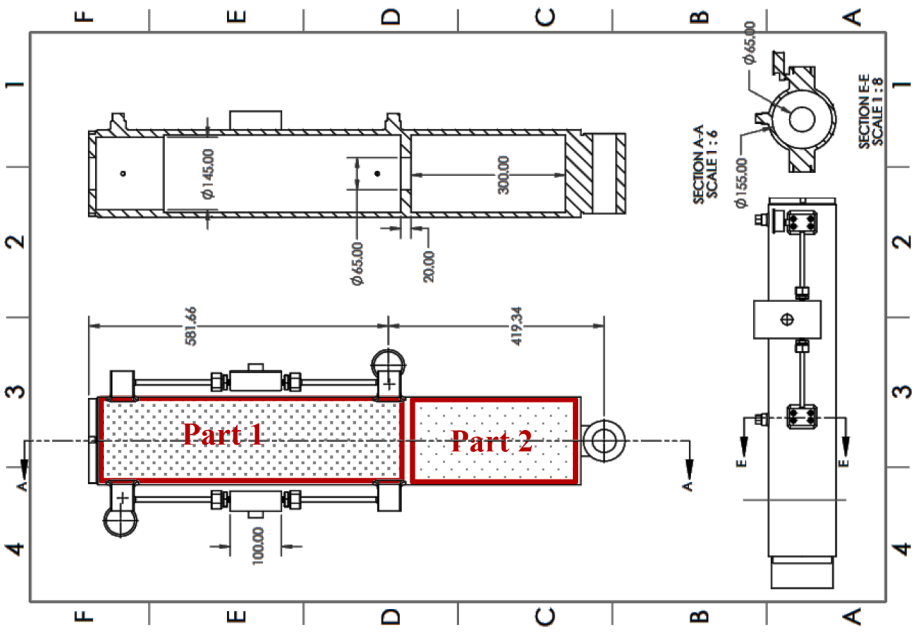

Fig. 9. Drawing of SABFD hydraulic cylinder.

Fig. 10. Fabrication of the hydraulic cylinder of the SABFD device.

Table 2
-Digital Motorized Valve specifications.

Type	Intelligent Type
Model	10
Torque Output	100 Nm
Body Material	SS304
Max Pressure	400 bar
Angle of Rotation	0-90°
Working Current	0.35 A
AC 220 V Drive Motor	75 W
Weight	5 kg
Intelligent Control Actuator (DC24V)	4–20 mA
Voltage	DC24V

and 3, respectively. The Gravitational acceleration, g is 9.8 m/s^2, and when the damper is installed horizontally, $z_1 = z_3$. Parameter, h_L, is total flow head loss, and is divided into two parts, major head loss, and minor head loss,

$$h_{L=}h_{Lmajor} + h_{Lminor} \tag{7}$$

The pressure drops inside the device due to passing fluid through elbows and valves are demonstrated by the minor, Equation (8), and major, Equation (9), head loss parameters.

$$h_{Lminor} = k_L \frac{{v_{pp}}^2}{2g} \tag{8}$$

$$h_{Lmajor} = f \frac{L_{pp}}{D_{pp}} \frac{{v_{pp}}^2}{2g} \tag{9}$$

where K_L is a minor head loss coefficient and is equal to 0.5 for Sharp-Edged entrance of the pipe, [14].

The parameter f is Friction Factor and can be defined according to geometrical parameters by the Blasius equation [3]. Accordingly, L_{pp} is pipe length, and D_{pp} shows pipe internal diameter. By computing the pressure inside the bypass pipe, the total pressure drop can be obtained. The damping coefficient of the damper device is demonstrated through Equation (10).

Fig. 11. Valve Screen, the command from PLC panel (Greenlight), valve feedback (Red light). (For interpretation of the references to colour in this figure legend, the reader is referred to the web version of this article.)

Fig. 12. Experimental test configuration.

Table 3
Digital pressure transducers specifications.

Housing	Stainless Steel (IP65, IP67)
Connection	threaded connection G 1/4 internal thread
Signal Output	: 4 ~ 20 mA
Wetted Part	1.4542 (17–4 PH / 630)
Power Supply	12 ~ 30VDC
Operation Temperature	−25 ~ 80C
Measuring Range	0 ~ 5800 psi

$$C = \left[\frac{\rho A_{cl}^3}{2A_{pp}^2}\right]\left[K_1 + K_f\right]v_{pp} \tag{10}$$

where $K_f = \frac{fl_{pp}}{d_{pp}}$, and K_1 is the loss coefficient and can be defined through Equation (11).

$$\frac{p_1 - p_2}{\rho} = \frac{1}{2}\left[1 + \frac{fL_{pp}}{D_{pp}}\right]V_{pp}^2 + K_1\frac{V_{pp}^2}{2} \tag{11}$$

Using Equation (11), for volume-2 and volume-3 for valve position (β) in the range of fully closed up to 85%, the pressure inside the pipe has been calculated and depicted in Fig. 4. It can be seen from this graph that when the valves begin to close from the fully open conditions, the upstream pressure inside the bypass pipe starts to rise. Whereas the pressure of downstream, after valves, drops. When β increases more than 75% and the opening of the valve is only 25 percent or less, the function of the device changes, gradually, start to work as a restrainer and the slope of the pressure curve increases dramatically. Therefore, it can be concluded that the SABFD device performance is more sensitive to the β if $\beta > 75\%$.

Accordingly, the damping coefficient parameter from Equation (10) can be computed for different values of β. The variations of the damping coefficient with β are illustrated in Fig. 5. From this curve, the function of C can be extracted as Equation (12).

$$C = -0.001\,\beta^3 + 0.4382\,\beta^2 - 3.5214\beta + 15.185 \tag{12}$$

Thus, the numerical computations predict the damping coefficient of the SABFD damper is raised with the increase of β. When the valve is almost closed, and β is bigger than 75%, damper function changes from the damper to a restrainer, so the damping coefficient gradually drops to zero at $\beta = 100\%$. Thus, it is predicted that the numerical calculations using damper equations do not apply for β higher than 75% and the damping force and damping coefficient should be extracted from Equation (13), from the pressure differences between chamber 1 and 2, and also from the experimental test outcomes.

$$F_{SABVD} = (A_{cl})^2 \bullet (p_2 - p_1) + A_{Shaft} \bullet p_2 \tag{13}$$

Where A_{Shaft} is the occupied cross-section area by the shaft. From Equation (13), the resultant force of the SABFD device is numerically predicted and depicted in Fig. 6. This graph estimates the damping performance of the device is also increasing with closing the valve.

4. The fuzzy logic control algorithm

The fuzzy logic control algorithm has been adopted in this study to control the action of digital motorized valves based on the displacement of the bridge deck measured via installed LVDT sensors and the pressure of fluid inside the bypass valve measured by the digital pressure transducer.

The employed fuzzy logic technique in this study is an open-loop control algorithm as shown in Fig. 7, and has been developed based on the predicted performance of the device and test equipment limitations at the structural laboratory as demonstrated in Table 1. To define fuzzy rules for real-time control of the structural system, three steps have been considered in which the displacements change from the Ultimate, Large and Small ranges. The Ultimate range has been considered for the displacements that may cause a surge in the viscous damper and pass the pressure safety limits. For the current experimental study, this limit has been considered to be equal to 17 mm (in both pull and push directions) regarding test equipment limitations. The large displacement is defining the displacements within a range that put the valve position at 90%. Whereas, the small displacements have been considered for β equal to 50%. With these fuzzy rules, it is predicted that when the displacement of the structure changes between these rages, the valve position varies automatically and changes the stiffness and damping coefficient of the device.

Thus, the resultant control force is a function of the valve position (β) and can be changed according to the structural displacement due to dynamic behavior. The open-loop control system is very economical because of its simplicity and stability. Nevertheless, due to the lack of a feedback system, it cannot eliminate the fluctuations and achieve the desired reduction in response.

Fig. 13. Setup of the PLC controller.

Table 4
PLC controller specifications.

processor	7″ HMI with IX runtime
Screen	TFT-LCD Touch Screen (800 × 480 pixel – 16:9)
memory	200 MB application memory
I/O section	Embedded PLC IO (8 × Digital Input, 4 × Digital Output) −1 pc of 4 channels Analog Input Card for 2 × Pressure Sensor Input −1 pc of 2 channels Analog Output Card for 1 × Motorized Valve Control
Power Supply	24VDC
Control Relay	24VDC × lot
Power	ABB MCB 6A / 2P / 6kA × 2

5. Fabrication of the prototype

The manufactured prototype of the SABFD control system which consisted of the bypass fluid damper and PLC controller is shown in Fig. 8. The prototype for the SABFD device has been fabricated according to the drawing of the hydraulic cylinder and bypass pipes as illustrated in Fig. 9.

5.1. Double action hydraulic cylinder

As can be seen in the drawing, the hydraulic cylinder consists of two parts. Part 1 is the main part of the cylinder in which the piston head movement inside Part 1 pushes and discharges oil from the hydraulic cylinder into the bypass pipe. The pressure changes inside Part 1 according to the valve position (β) and the excitation displacement. The second part, which is labeled Part 2, is the isolated space that is considered only to make sufficient space for the shaft and shaft end-head to move. This part added to the configuration of the conventional hydraulic cylinder to make identical volume for the shaft to occupy in both chambers for equal double action of the cylinder. This part of the cylinder is considered to be sealed to avoid any leaking. These two parts of the hydraulic cylinder are shown in Fig. 10 during the manufacturing process.

5.2. Controllable Digital Motorized Ball Valves

The Digital Motorized High-Pressure Ball Valve which has been implemented in this study is able to persist up to a maximum pressure of 400 bar and can change between 0° (fully open) to 90° (fully close) position to control the fluid flow between two chambers through bypass pipes during movement of shaft and piston. The detailed characteristics of the digital ball valves are listed in Table 2. The valves screen can be seen in Fig. 11. In this screen, both the PLC command (green light) and the valves' feedback (red light) can be observed.

5.3. Digital pressure transducers

Two digital pressure transducers have been placed on the hydraulic cylinder to measure the pressure of both chambers of the hydraulic cylinder during the operation of the damper device. The position of the pressure sensors is considered at both ends of the cylinder to record all the pressure variations during the pull and push excitations (Fig. 12). The specifications of the pressure transducers are listed in Table 3.

5.4. Programmable logic controller

The PLC controller screen and other components are demonstrated in Fig. 13. The PLC controller is comprised of a mainboard, processor, memory, screen, power supply, and an Input/Output section for 8 Digital Input and 4 Digital Output which are installed inside the metal enclosure with the size of 500 mm in height, 400 mm in width and 200

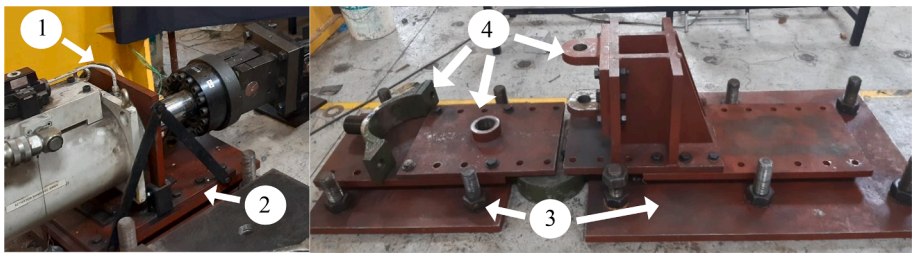

Fig. 14. Experimental test support and restrainers: (1) Actuator back support, (2) Actuator uplift restrainer, (3) Damper uplift restrainer, (4) Damper back rigid support.

Fig. 15. The SABFD device experimental test set-up.

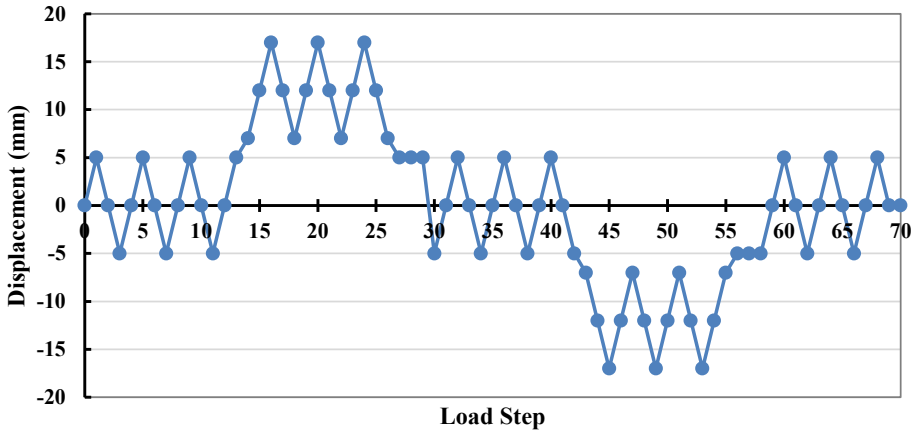

Fig. 16. Applied displacement during real-time control.

mm in Depth. The processor is equipped with the internal HMI System (IX Beijer) for data programming. The detailed specifications of the PLC controller are listed in Table 4.

The analog input module has been used to connect and receive data from Digital Pressure transducers and the analog out module has been used to connect and send commands to Digital Motorized Valves.

The special program has been coded for the PLC and all required commands were regulated through the predefined fuzzy control algorithm.

The PLC controller receives the data related to the displacement through LVDT sensors and also fluid pressure data through digital pressure gauges and then determines the appropriate valve position corresponding to the required damping force to minimize bridge movement. The determined valve position is sent as a command to the motorized valves to change and adapt the function of the fluid damper device to perform a real-time control on the bridge displacement. The motorized valve starts to regulate the valve position after receiving the command. Data regarding any changes in the valve position resends to the PLC controller as device feedback.

Since with increasing the displacement of the structure, the required resistance force increases, ultimate displacements may occur during the operation that causes a surge in the viscous damper and pass the pressure safety limits. For this reason, a pressure release command on the panel has been applied to avoid over-limit pressure inside the hydraulic cylinder for safety purposes. Several experimental tests including incremental cyclic tests and cyclic load frequency tests have been conducted to assess the performance of the SABFD prototype.

5.5. *Testing setup*

The test setup was included four main parts to align the prototype with the dynamic actuator and also fix the end of the device to restrain vertical movement. The installed set-up on the strong floor in the structural laboratory is illustrated in Fig. 14. In this configuration, back rigid support (Part 1) and uplift restrainer (Part 2) hold the actuator, and Parts 3 and 4 have the same function of holding the prototypes and aligning them with the actuator.

The horizontal Shimadzu dynamic actuator with 300kN load capacity, a 4830-model servo controller, and a 110-liter hydraulic pump has been utilized to apply the dynamic excitation to the device during manual and automatic control tests.

Fig. 15 (a) shows the installed prototype of the SABFD in the test setup. While the connection of the SABFD damper to the PLC controller has been demonstrated Fig. 15 (b).

6. Experimental test of the semi-active control system

To evaluate the semi-active control system, both incremental cyclic and cyclic load frequency tests have been conducted. For these experiments, a horizontal electro-hydraulic actuator was used to implement a saw-tooth displacement pattern, shown in Fig. 16. To evaluate the damper device accurately, three or more cycles of loading were applied

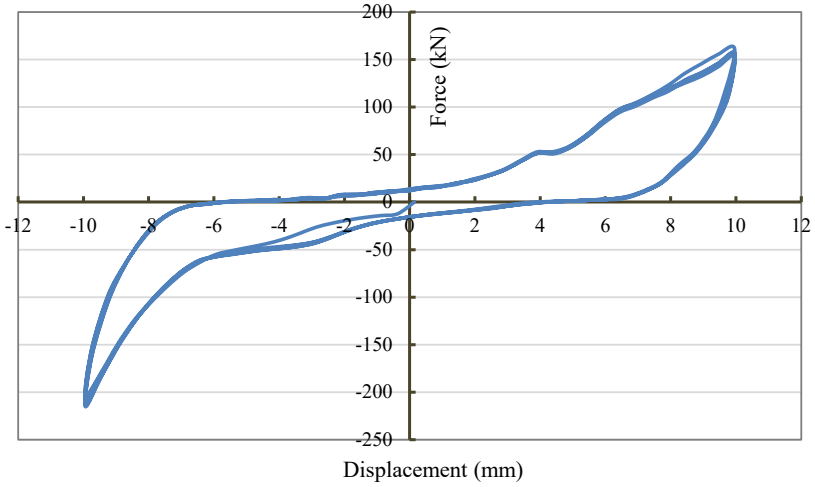

(a) Manual control of β=70%

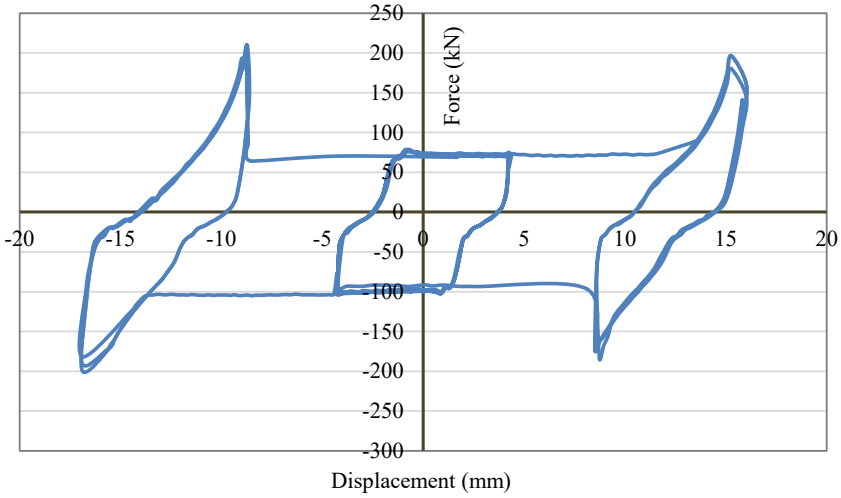

(b) Real-time control excitation time-step =5 sec

Fig. 17. Force-displacement time history.

Table 5
Defined characteristics of the SABFD device.

β (%)	0	50	75	87.5	100
C (N.s/mm)	16.5	816	1666	2203	0
K (N/mm)	33	833	2000	3333	25,000

at a predefined condition [9].

The maximum applied displacement is defined based on the actuator limitations and safety protocols so that the maximum generated force by the device stays less than 100 kN. In between the maximum range of pull and push, two different steps have been considered to check the performance of the device through automatic control. The incremental displacement pattern begins with a small displacement of 5 mm in both negative and positive directions (Pull and push). While the displacement is below 5 mm the valve position is set to β = 70% which means the valve is only 30 percent open and the SABFD device is assumed to function to dampen the vibration energy. After 10 s as the excitation displacement increases up to 17 mm, the control system is programmed to set the valve position to β = 90% which will close the valve up to 15 percent. In between of steps of applying displacement to the device, a three-step rest has been considered while valves go from a closed position to the open state. These rest gaps are applied to the test to prevent the temperature rise and also to compensate the valve delay and allow the valves to be set to the previous command value. The movement of the piston head during the test is measured by one LVDT sensor. The LVDT outputs were imported to the PLC controller as a PLC input, and then, the panel calculates the valve position based on the predefined fuzzy control rules.

The incremental displacements have been applied with the time steps of 5 s in the first test. And then the time decreased to 3 sec and 1 sec, respectively. These variations were applied to examine the function of the control system according to excitation velocity. It is worth mentioning that the motorized valves required 13 s to change 90° from totally open position to totally close status.

6.1. *Incremental cyclic test results*

To check the damping performance of the SABFD device through real-time control, firstly, a 10 mm displacement was applied to the device while the valve position was set to 70% manually and the output was recorded as it can be seen in Fig. 17(a). In this condition, the SABFD device functioned as a damper with a damping coefficient of about 620

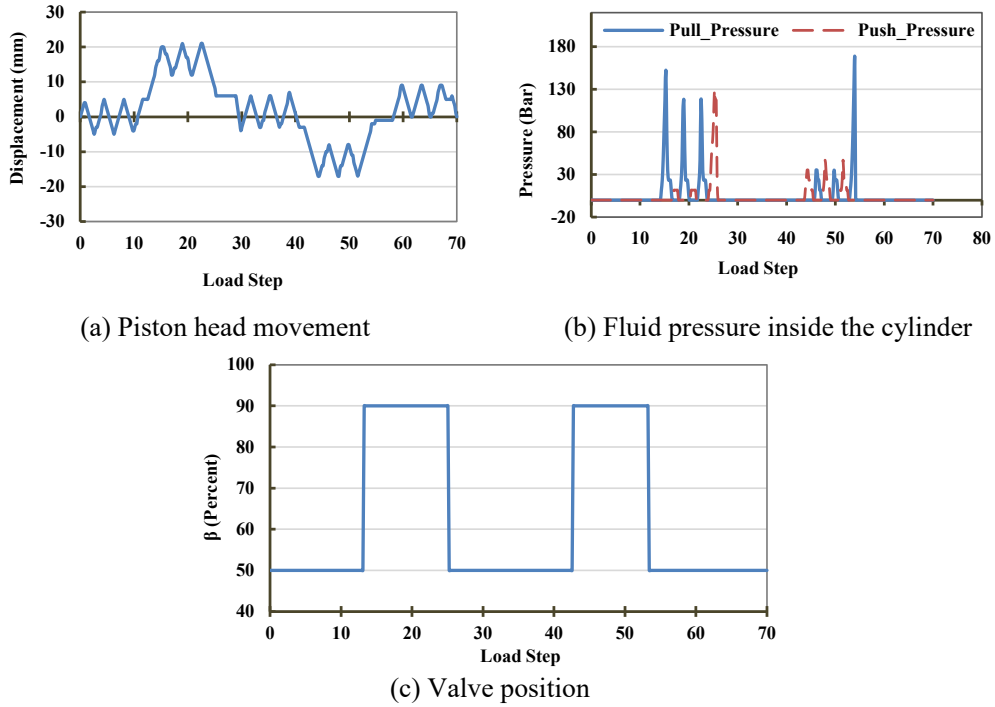

(a) Piston head movement (b) Fluid pressure inside the cylinder

(c) Valve position

Fig. 18. Recorded data during real-time control.

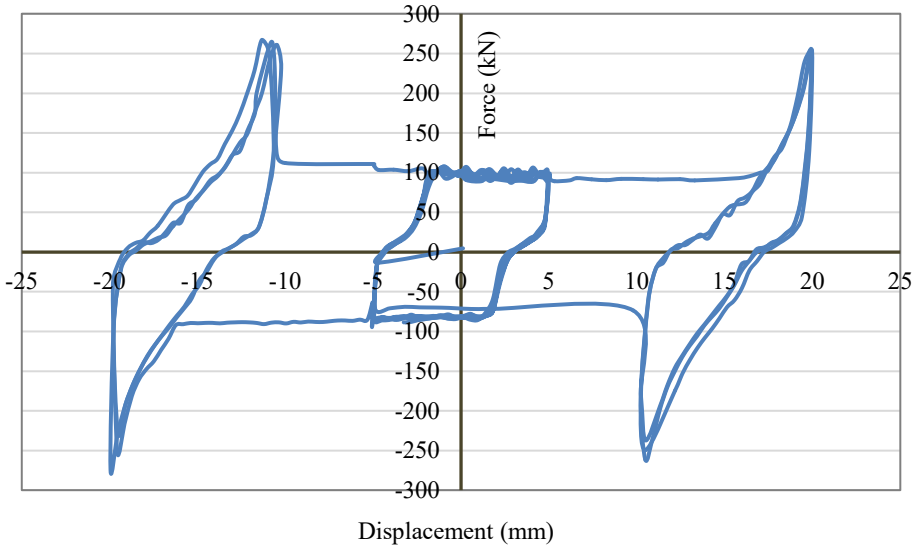

Fig. 19. Force-displacement time history for excitation time-step = 3 sec.

N.s/mm. This procedure repeated for β equals 0, 50%, 75%, 87.5%, and 100%, and the damping coefficient and stiffness of the device extracted from the experimental tests and listed in Table 5.

For the next step, a real-time control has been tested while displacement protocol was applied according to the displacements in Fig. 16 and the control rules were applied by the PLC controller. To record the force–displacement time history data, the force values have been measured through the actuator data acquisition system, and the displacements were recorded by PLC from the LVDT sensor. The force–displacement curve is demonstrated in Fig. 17(b).

The recorded data by PLC during the test (displacement, pressure, and valve position) are shown in Fig. 18(a), (b), and (c), respectively. It can be seen from the graph in Fig. 18(c) that the valve position has been changed during the test according to the displacement variations. Changes in the valve position have varied damping and stiffness characteristics of the device so that the hysteresis loop shifted along the displacement axis (x-axis).

During the experimental test, always there are two different values for the valve positions. The command value was an output data of the PLC and the value of the valve feedback. A time delay due to the valve speed made the real valve position (feedback) different from the commending value. This difference increased when the velocity of the applying force was raised.

Fluid pressures inside the SABFD device in both chambers of the hydraulic cylinder were the other parameters that were measured and recorded by the PLC controller during the experimental tests.

These values have been shown in Fig. 18(b). As it can be seen in the graph, during the pull and push, the pressure of the fluid raised to 170

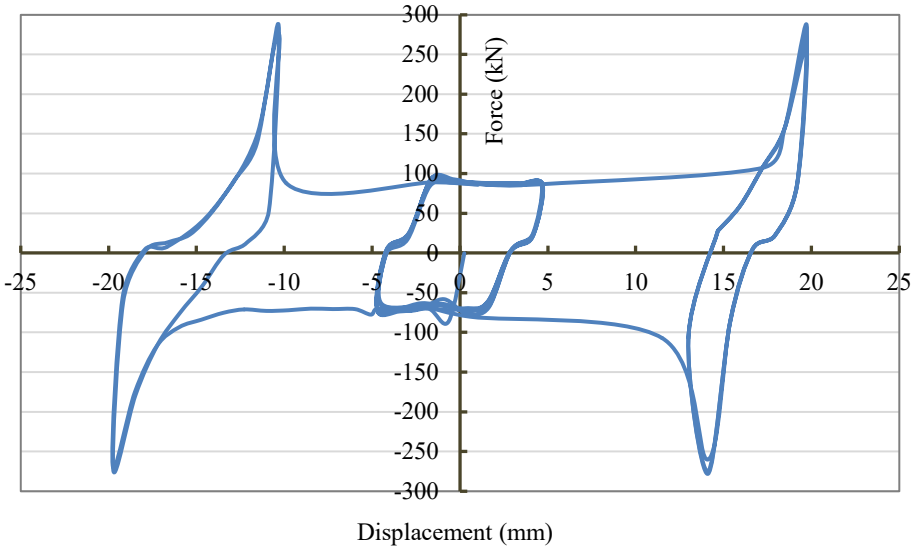

Fig. 20. Force-displacement time history for excitation time-step = 1 sec.

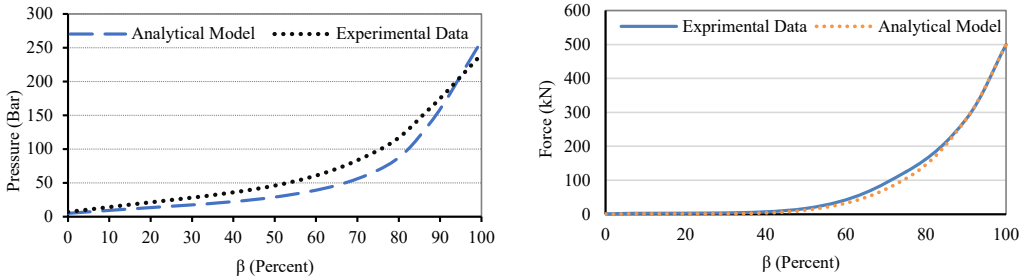

(a) pressure (b) Resultant force

Fig. 21. Data Validation.

Bar when 17 mm displacement was applied to the device.

6.2. Cyclic load frequency test results

To examine the dependency of the performance to the velocity of the excitation load, a series of experimental tests have been conducted on the device and the results have been recorded.

Fig. 17 shows the force–displacement history curve while the time steps for applied displacements have been considered equal to 5 s. The valve positions (β), shown in Fig. 18 (c), have been changed between 50% and 90%. These two command values are outputs of the control system but the real valve position always was changing between these two values.

Afterward, to increase the load frequency, each time step has been set to 3 s and the experimental test has been repeated. During all the tests maximum force was limited due to the test equipment limitations. As a result, by changing the time steps of loading from 5 sec to 3 sec the resistance force of the device improved by 20%.

Fig. 19 demonstrates the outcomes of this step of the test. When the excitation load velocity raises, the delay of real β, in comparison with the commend value, increases. To check the device performance accurately, the time step decreased to 1 s for the next step and the test results are depicted in Fig. 20. As it can be seen in the graph, the time step change from 3 sec to 1 sec increases the resistance force up to 280 kN.

This test revealed that although the resultant force is increased and the performance of the device improved when the velocity of the excitation load increases, but the valve speed and delay can affect the resultant performance and the hysteresis loop, significantly. The control algorithm for all these tests was considered to be the same and the valve command positions were 50 for the displacements below 7 mm and 90 for the displacements more than 7 mm. But with increasing the force–velocity the difference between the command and real value position has been raised.

6.3. Validation of numerical result with experimental test

To validate the experimental and analytical outcomes, the observed pressure data during the tests were compared with the numerical calculations. The results are depicted in Fig. 21(a). Comparison of the two curves shows the pressure inside the cylinder varies gradually when β is smaller than 75% and then the slope of the pressure-β curve is increasing dramatically. The overall resultant force is illustrated in Fig. 21(b) for both analytical and experimental approaches. the results revealed a promising agreement between the data from the analytical model and experimental tests. For valve closing more than 75% percent, $\beta \geq 75\%$, the overall behavior of the SABFD device varies from damper to the restrainer.

The validated model for the SABFD system, in the next step, is implemented to develop the finite element code for dynamic analysis of a bridge structure equipped with a supplementary SABFD device. This finite element code is utilized to evaluate the performance of the implemented device in the bridge structures between the pier and deck. The SABFD device functions to dissipate dynamic energy from the passing vehicles and increase the operational life of the bridge.

Lebuhraya Pulau Indah bridge in Malaysia

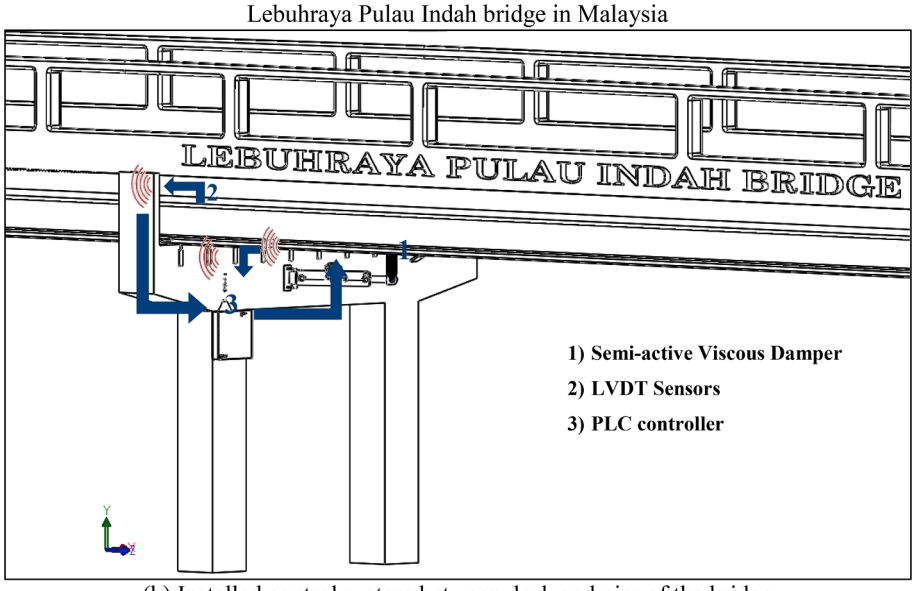

(b) Installed control system between deck and pier of the bridge

Fig. 22. The Integrated Adaptive Vibration Control System installed on the bridge structure.

Table 6
SABFD damper device geometrical parameters.

Cylinder			Pipe		
Length (m)	Diameter (m)	Thickness (m)	Length (m)	Diameter (m)	Thickness (m)
0.976	0.175	0.0125	0.8	0.0254	0.0218

Table 7
Mechanical properties of the fluid.

Density (15 °C)	0.88
Relative Vapor Density (air = 1)	>1
Viscosity	65 mm^2/s@40 °C

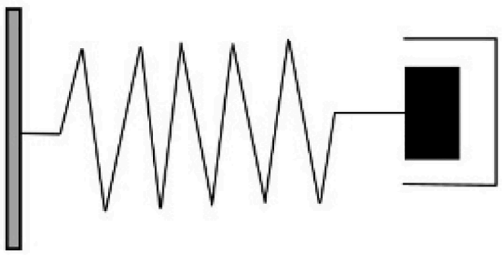

Fig. 23. Maxwell Model.

7. Application of developed Integrated Adaptive vibration control system in the LEBUHRAYA PULAU INDAH bridge

The developed Integrated Adaptive Vibration Control System has been implemented to the LEBUHRAYA PULAU INDAH bridge which is located in Kuala Lumpur, Malaysia, in order to evaluate the performance of SABFD according to applied traffic loads. The bridge and the model are illustrated in Fig. 22 (a). The schematic diagram of the installed Integrated control system in the bridge is depicted in Fig. 22 (b). The pressure inside the viscous damper is measured and recorded during the function of the device for safety purposes.

Since a series of experimental tests were conducted on the prototype of the device, the geometry, boundary condition, and material specifications of the device, have been defined according to the design of the prototype for testing by using a hydraulic jack. So, the geometrical and mechanical parameters of the hydraulic cylinder and hydraulic fluid have been defined according to the availability of material, production, and test limits. Dimensions of the SABFD hydraulic cylinder, bypass pipes, and oil mechanical properties are listed in Table 6 and Table 7 respectively.

According to the limitation of the test equipment, the maximum excitation force has been considered to be equal to 300 kN. For analytical prediction and experimental testing, the temperature is set to 30 degrees Celsius, which is the same as the ambient temperature. However, to maintain the desired temperature during the experimental test, sufficient rest time has been considered in between each cycle test to avoid any temperature rise.

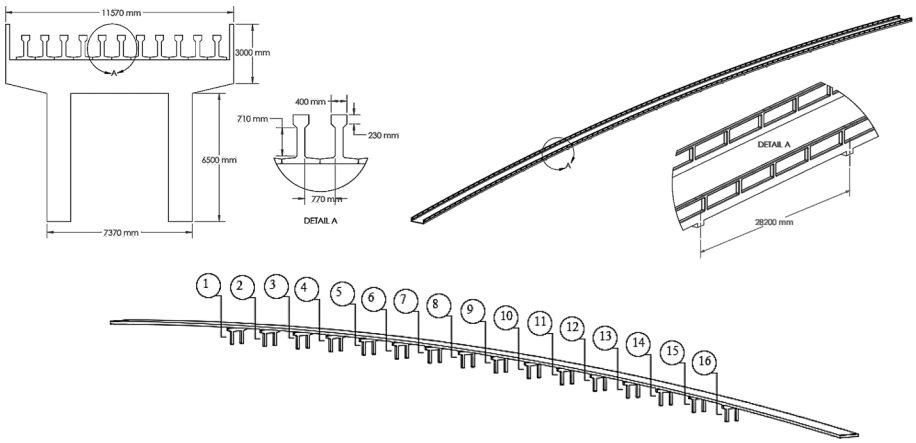

Fig. 24. Lebuhraya Pulau Indah bridge configuration.

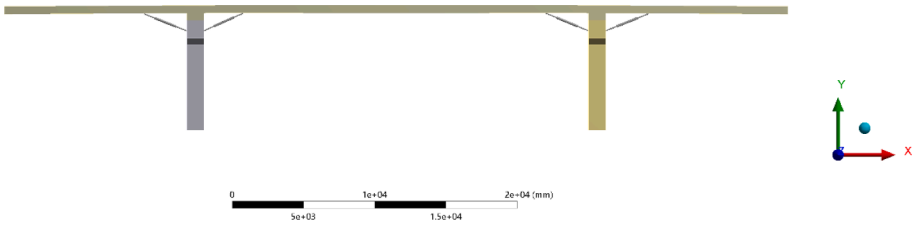

Fig. 25. Middle span of the bridge equipped with SABFD dampers.

Table 8
Fuzzy control rules.

B (%)	Displacement	Logic	Fuzzy Rule	C	K
100	x > 2.2 mm	Or	y > 12 mm	0	25,000
87.5	2.2 mm ≥ x > 2 mm		12 mm ≥ y > 8 mm	2203	3333
75	2 mm ≥ x > 1.8 mm		8 mm ≥ y > 6 mm	1666	2000
50	1.8 mm ≥ x > 1.5 mm		6 mm ≥ y > 4 mm	816	833
0	1.5 mm ≥ x		4 mm ≥ y	16.5	33

Table 9
Traffic loading on the bridge.

Loading Class	Loading per Lane (kN/m)	Total Load (kN/m)
H20	29.66	118.64
H15	22.245	88.98
H10	14.83	59.32
HS20	32	128
HS15	24	96

8. Development of finite element program for modeling and analysis of semi-active control of a bridge equipped with SABFD device

A dynamic response study of the real-time control system is very critical for determining the effect of the dampers on the overall response of the structure. Analysis of the dynamic response requires simulation of the structure and dampers at the same time.

8.1. Bridge-damper finite element model

To develop the finite element model of the bridge-damper, the Newton Raphson method, along with implicit numerical integration methods were utilized to provide a solution of the nonlinear system. The analysis has been done using the commercial software ANSYS 2019 R1. To define the dynamic and structural parameters of the SABFD damper the Maxwell model has been used through implementing spring elements by assuming that the properties can be represented by a spring and a dashpot connected in series. The schematic diagram of the model is shown in Fig. 23 [2,12]. The model considers both the elastic (K), spring, and the viscous moduli (C), dashpot, of the damper. In the Maxwell model, the elastic stress in the spring and the viscous stress in the dashpot is the same, whereas the strain of the system is the sum of the individual strains.

Since the fatigue issue in mechanical parts of the bridge number 015/61 located in LEBUHRAYA PULAU INDAH, has been reported by the Ministry of Works Malaysia (Jabatan Kerja Raya, JKR), which is responsible for construction and maintenance of public infrastructure, the has been considered to analysis and a finite element model of the bridge equipped with SABFD devices has been developed. The bridge configuration is demonstrated in Fig. 24.

To control the bridge vibration due to the traffic loads, two SABFD dampers have been considered to be installed in each span between the piers and the deck of the bridge. The installed SABFD devices for the middle span of the bridge are demonstrated in Fig. 25.

To analyze the bridge four traffic load conditions have been considered according to The American Association of State Highway and Transportation Officials standards [1]. These load conditions include minimum and maximum traffic loads and two allowable vehicle speeds. The bridge consists of 15 spans, each span length of 28.2 m, so to analyze the middle span of the bridge, a symmetry boundary condition is applied to both ends of the model in Fig. 25.

To solve the nonlinear model of the bridge-damper, a Newmark method has been used. In this method, if u_t denotes for displacement vector, $\dot{u}_t$, for velocity vector, and $\ddot{u}_t$ for acceleration vector, considering the equation of motion for the equivalent viscously damped case is given by:

$$M\ddot{u}_t + C\dot{u}_t + Ku_t = F_t \tag{14}$$

where K is stiffness matrix, M is mass matrix and C is damping matrix, and through shortening Taylor's series, the following equations can be

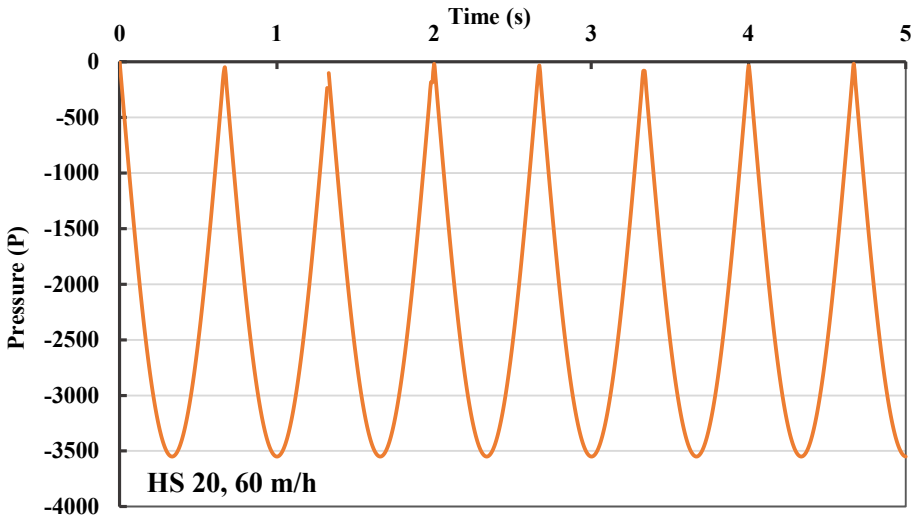

Fig. 26. Traffic load pattern for maximum traffic and maximum vehicle speed.

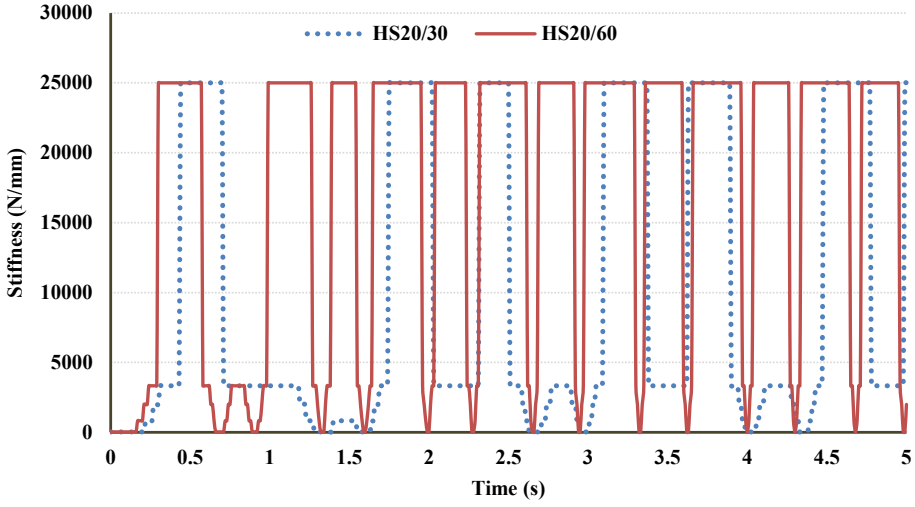

Fig. 27. The variations of stiffness during HS20 loading condition.

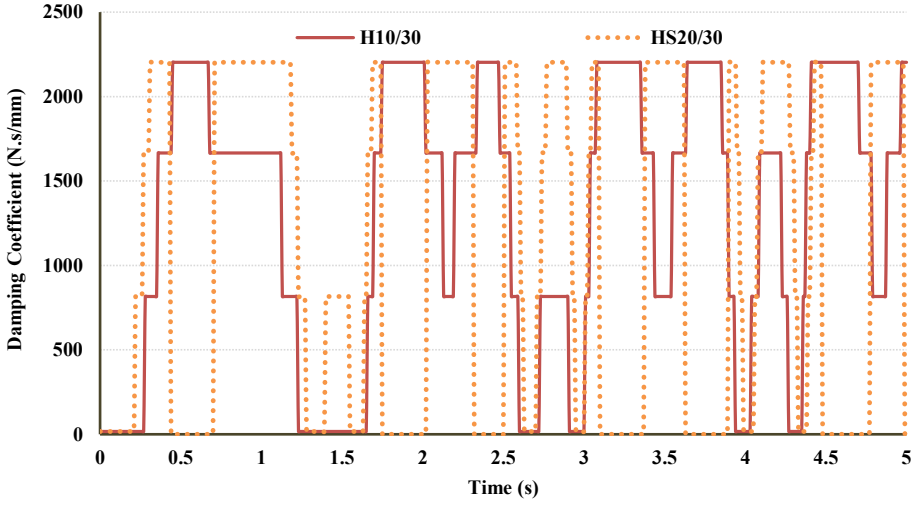

Fig. 28. Variations of dampers' damping coefficient subjected to traffic speed of 30 mile/hour.

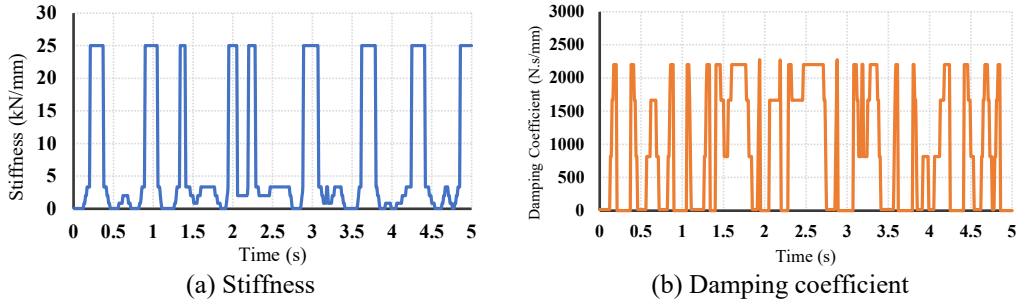

Fig. 29. SABFD parameters variations during real-time control.

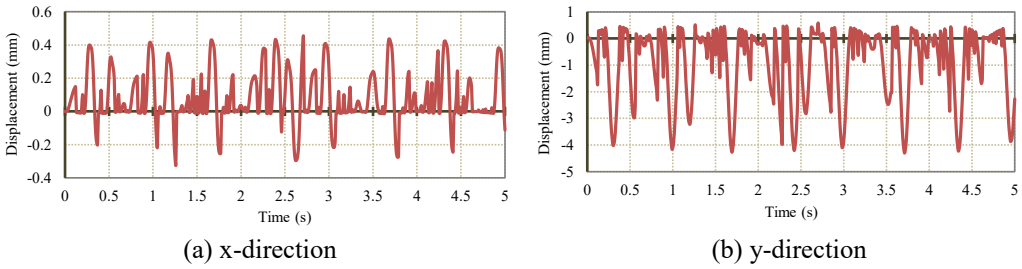

Fig. 30. Midspan displacement during real-time control.

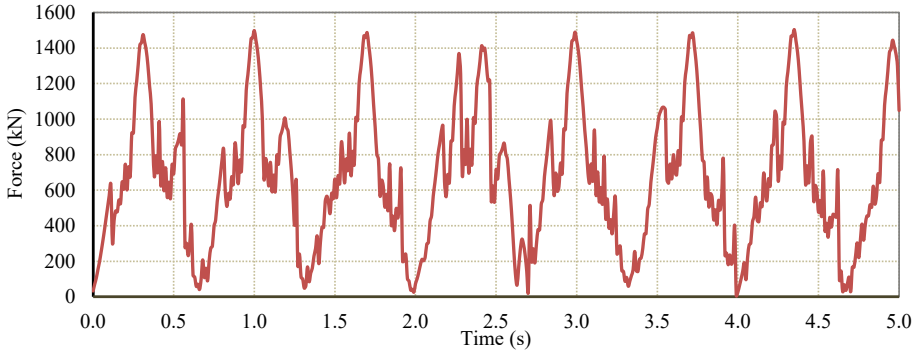

Fig. 31. Pier reaction force during the analysis with real-time control.

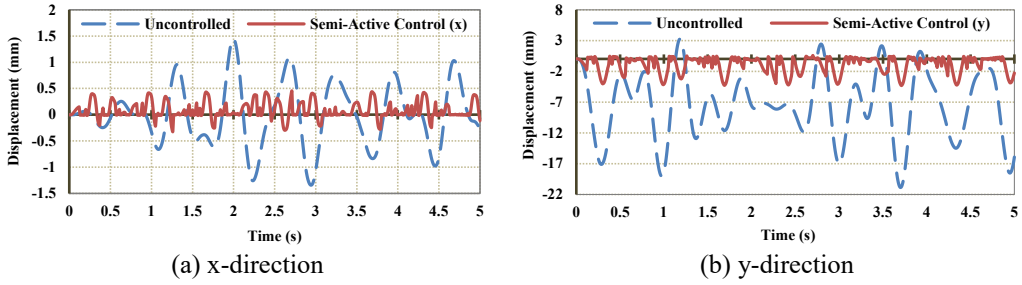

Fig. 32. Real-time control response of the bridge in comparison with uncontrolled structure, mid-span displacement.

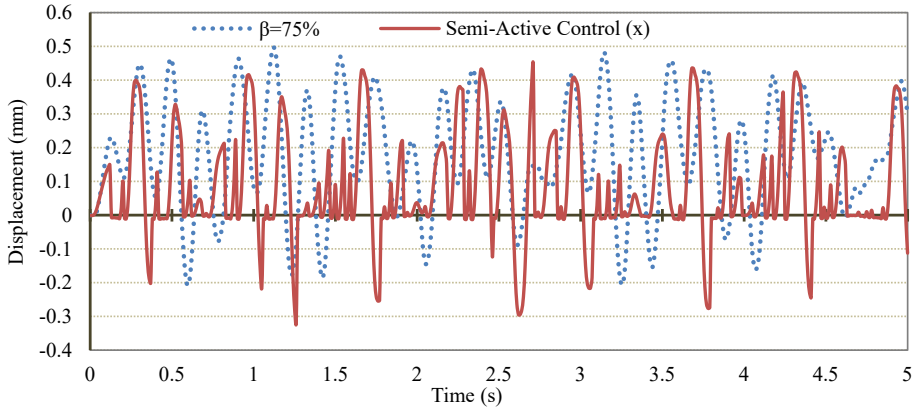

Fig. 33. Real-time control response of the bridge in comparison with β = 75%, mid-span displacement in the x-direction.

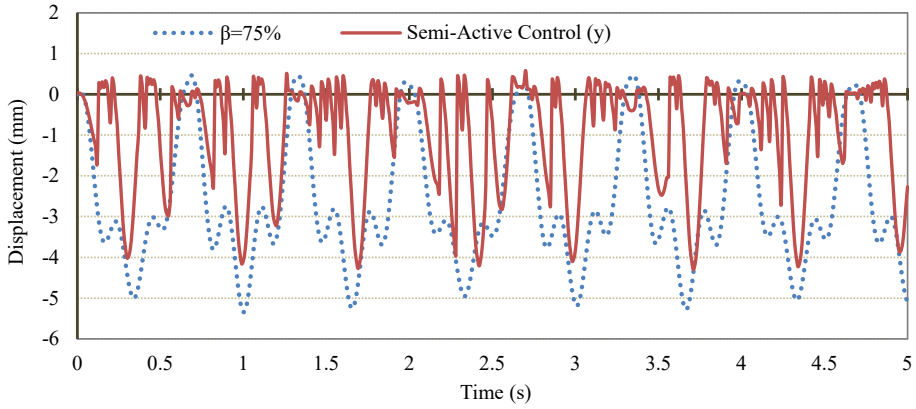

Fig. 34. Real-time control response of the bridge in comparison with β = 75%, mid-span displacement in y-direction.

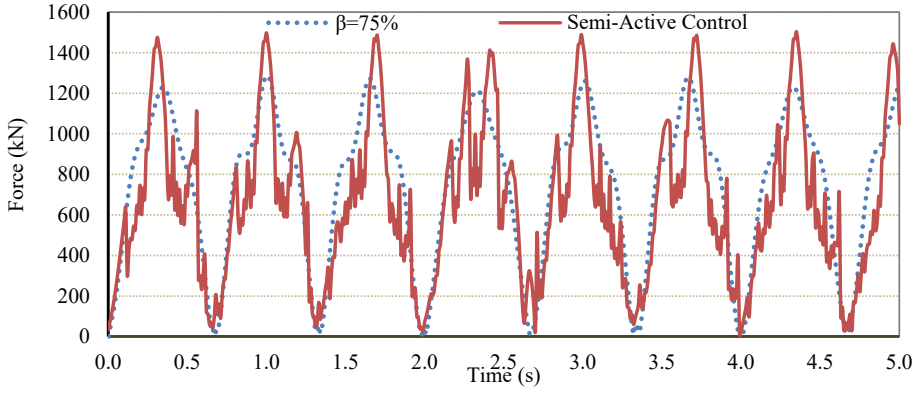

Fig. 35. Pier reaction force during Real-time control.

written:

$$u_t = u_{t-\Delta t} + \Delta t \dot{u}_{t-\Delta t} + \frac{\Delta t^2}{2}\ddot{u}_{t-\Delta t} + \beta \Delta t^3 \dddot{u} \tag{15}$$

$$\dot{u}_t = \dot{u}_{t-\Delta t} + \Delta t \ddot{u}_{t-\Delta t} + \gamma \Delta t^2 \dddot{u} \tag{16}$$

Therefore, Equation (16) can be written in the case of linear acceleration within the time step,

$$\dddot{u} = \frac{\left(\ddot{u}_t - \ddot{u}_{t-\Delta t}\right)}{\Delta t} \tag{17}$$

The standard form of Newmark's equations obtains by substitution of Equation (18) into Equations (16) and (17),

$$u_t = u_{t-\Delta t} + \Delta t \dot{u}_{t-\Delta t} + \left(\frac{1}{2} - \beta\right)\Delta t^2 \ddot{u}_{t-\Delta t} + \beta \Delta t^2 \ddot{u} \tag{18}$$

$$\dot{u}_t = \dot{u}_{t-\Delta t} + (1-\gamma)\Delta t \ddot{u}_{t-\Delta t} + \gamma \Delta t^2 \ddot{u} \tag{19}$$

Since, the Newmark method utilizes finite-difference expansion for the time interval, Δt, the solution for Equations (19) and (20) are computed by iteration for each time step for each displacement DOF of the structural system. By using matrix notation [30], the solution for the displacement at time t is obtained by deducing the equations (3.1.5) and

Table 10
Reduction factor for span subjected to different load conditions in comparison with bare structure response.

H 10 /30 Max Response Reduction Factor (%)	50	75	100	Real-time Control
Displacement x-Direction	14.3	42.9	57.1	50.0
Displacement y-Direction	45.9	73.0	73.0	78.9
Reaction force	16.9	26.0	−5.2	8.3
HS 20 /60 **Max Response Reduction Factor (%)**	**50**	**75**	**100**	**Real-time Control**
Displacement x-Direction	58.6	66.2	71.0	69.0
Displacement y-Direction	65.0	74.4	79.1	79.4
Reaction force	7.7	19.5	−7.8	5.9
H 10 /60 **Max Response Reduction Factor (%)**	**50**	**75**	**100**	**Real-time Control**
Displacement x-Direction	39.8	56.6	72.3	50.6
Displacement y-Direction	51.5	74.8	75.8	81.1
Reaction force	20.1	28.9	−0.8	19.0
HS 20 /30 **Max Response Reduction Factor (%)**	**50**	**75**	**100**	**Real-time Control**
Displacement x-Direction	12.0	40.0	60.0	36.0
Displacement y-Direction	30.7	65.4	80.5	72.8
Reaction force	5.5	15.8	20.1	14.5

(3.1.6) from equations (19) and (20):

$$\ddot{u}_t = b_1(u_t - u_{t-\Delta t}) + b_2\dot{u}_{t-\Delta t} + b_3\ddot{u}_{t-\Delta t} \tag{20}$$

$$\dot{u}_t = b_4(u_t - u_{t-\Delta t}) + b_5\dot{u}_{t-\Delta t} + b_6\ddot{u}_{t-\Delta t} \tag{21}$$

where the constants b_1 to b_6 are computed in the solution procedure.

$$b_1 = \frac{1}{\beta\Delta t^2} b_2 = \frac{1}{\beta\Delta t} b_3 = \beta - \frac{1}{2}$$

$$b_4 = \gamma\Delta t b_1 \quad b_5 = 1 + \gamma\Delta t b_2 \quad b_6 = \Delta t(1 + \gamma b_3 - \gamma)$$

The substitution of Equations (20) and (21) into Equation (14) forms the dynamic equilibrium of the system at a time "t" to be written in terms of the unknown node displacements u_t.

$$(b_1M + b_4C + K)u_t = F_t + M\left(b_1u_{t-\Delta t} - b_2\dot{u}_{t-\Delta t} - b_3\ddot{u}_{t-\Delta t}\right) + C\left(b_4u_{t-\Delta t} - b_5\dot{u}_{t-\Delta t} - b_6\ddot{u}_{t-\Delta t}\right) \tag{22}$$

Thus, to solve the dynamic equations of the system, the integration constants are computed from the static stiffness matrix K, mass matrix M and damping matrix C, in the first step. Then according to the initial condition, effective load, stiffness, and damping matrixes, as well as displacement, velocity, and acceleration vectors are calculated. Afterward, the calculation process is repeated for each time step. The Newton–Raphson method is also added to the model to update the stiffness matrix in nonlinear problems.

To conduct the real-time control on the bridge-damper structural system, the fuzzy algorithm code has been implemented in the finite element model of the bridge. The fuzzy control code is changing the stiffness and damping coefficient of the spring-dashpot model of the SABFD devices during the dynamic analysis based on the fuzzy logic in Table 8. These changes have been applied according to the calculated nodal displacements of the mid-span node at the previous load step. The index displacements have been predefined as the displacements of the middle span node in two vertical, y, and longitudinal directions, x, shown in Fig. 25.

To develop fuzzy rules, allowable horizontal displacement of the midspan is considered to be less than 50% of rubber strain, rubber thickness [31]. While allowable vertical displacement in the downward direction is less than compression limits of rubber bearings and in the upward direction is less than debonding limit of rubber bearings with steel plates in out of plane tensile. [19].

8.2. Development of the harmonic force model for moving traffic loads

The minimum and Maximum loads according to The American Association of State Highway and Transportation Officials (AASHTO, 1996) standards for bridges and highways have been summarized in Table 9. In this study, a loading condition of HS20 has been considered which assumes a loading of 32 kN/m per lane. Since the bridge has 4 lanes, the total load is considered to be 128 kN/m for each span of the bridge.

The passing vehicles have been assumed to pass the bridge with two different speeds of a maximum of 60 miles per hour (96.5 km/h) and a minimum of 30 miles per hour (48.2 km/h) according to the American Association of State Highway and Transportation Officials. Length of truck for all conditions considered to be maximum 20 m. The frequency of the harmonic load is calculated by assuming that the traffic load, which consists of truck weight and length parameters according to the HS20 conditions in the ASSHTO standard, passes the span length. The computed frequencies for 30 and 60 miles/hour are 0.37 to 0.75 Hz, respectively. Fig. 26 shows the harmonic traffic loads pattern for maximum traffic load, HS20, and maximum vehicle speed, 60 miles per hour, which was applied on the bridge deck.

The other three loading scenarios with different traffic loads and different vehicle speeds are also calculated. In this study, H10 denotes the minimum traffic load and HS 20 denotes the maximum traffic load scenario, according to ASSHTO standard code.

The variations in the stiffness of the dampers during the analysis of the bridge-damper structure have been compared in these different loading conditions. In Fig. 27, the traffic load of the bridge has been considered to be identical and equal to the maximum traffic scenario, H20, but the speed of the vehicles changed. Therefore, the frequency of the dynamic load varied from 0.37 to 0.75 Hz. In these two-loading conditions, the maximum traffic load applied to the structure and the displacement of the structure in the x and y directions are large. So, the function of the device changes to the restrainer frequently, to limit the extensive displacements.

On the other hand, in the following graph, Fig. 28, variations of the damping coefficient of the dampers have been illustrated while the speed of the vehicles is considered to be fixed and the loading conditions have been changed.

9. Results and discussion

To analyze the bridge, the maximum traffic load, HS20 loading condition, and maximum speed, 60 miles per hour, have been considered. The traffic load has been distributed on the bridge deck as a harmonic loading as is demonstrated in Fig. 26. For this purpose, the fuzzy control algorithm has been compiled and added to the finite element model of the bridge. The results show adding the damper to the structural system has a significant effect on mitigating the vibration of the mid-span node.

After applying the real-time control to the finite element model of the bridge-damper, the calculated stiffness values are changing during the analysis as can be seen in the graph in Fig. 29(a). Also, the damping coefficient of the SABFD device variations was depicted in the graph in Fig. 29(b).

The resultant displacement of the node at the mid-span in the x-direction is depicted in Fig. 30(a) and shows that the maximum displacement decreases up to 68%. For the y-direction also the control system functions properly and mitigates the displacement to values less

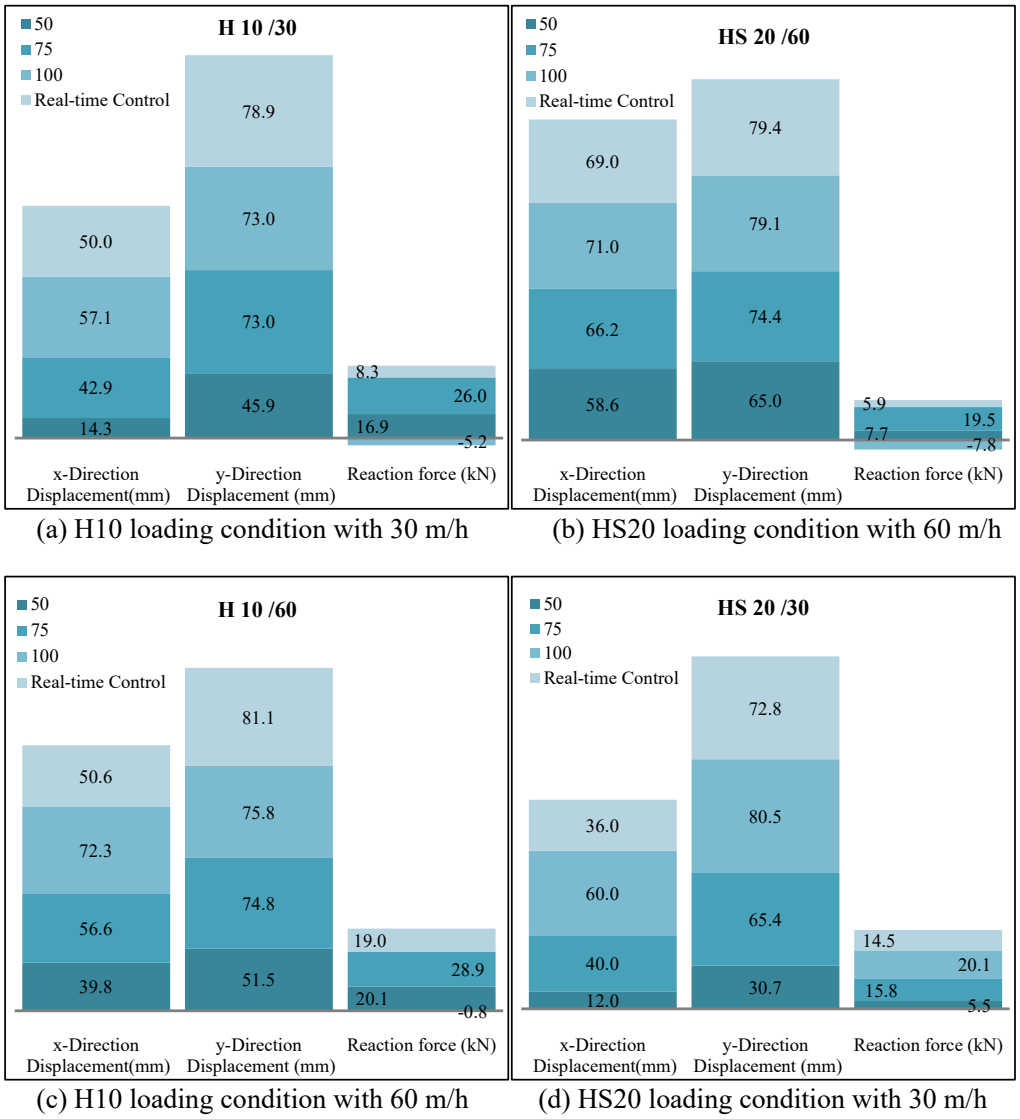

(a) H10 loading condition with 30 m/h (b) HS20 loading condition with 60 m/h

(c) H10 loading condition with 60 m/h (d) HS20 loading condition with 30 m/h

Fig. 36. Reduction Factor in different traffic load scenarios.

than 4.3 mm from 20.87 mm for bare structure (Fig. 30(b)).

During the real-time control of the bridge-damper structure, there is a harmonic change in the reaction force at the pier of the bridge with a maximum value of 1503 kN (Fig. 31).

The effectiveness of the control system can be proven by analyzing the curves Fig. 32(a). Where the bare structure responses have been compared to a controlled structure. From this figure, it is proven that the displacement of the bridge completely is restricted in the x-direction by the mean of the control system. The same performance is seen in the y-direction in Fig. 32(b).

To compare the manual and semi-active control systems, the displacements in the x-direction are depicted in Fig. 33 when the real-time control system is activated and when it is disabled and β is set to 75% manually. Results reveal that during loading, at some points the displacement values by manual control are less than automatic control and at some point, the response phase of the structure changed. But the overall behavior of the structure improved. In addition, it is worth mentioning that the maximum displacement values in the control algorithm were predefined and can be changed according to the required structure response. The same comparison in the y-direction demonstrates compatible results in Fig. 34.

The force reaction at the pier of the bridge in real-time control and manual control conditions is shown in Fig. 35. The result shows by applying the real-time control on the bridge-damper structure, although the overall reaction force is less than the manual control, through $\beta = 75\%$, at the time steps that overall displacement is maximum and the control system regulates β equal to 100% the reaction force raised and becomes more than the manual control through $\beta = 75\%$. This increase is still less than the maximum reaction force at manual control through $\beta = 100\%$ and it is closed to the bare structure response.

The numerical outcomes of the bridge middle span subjected to four discussed traffic loads are summarized and compared in Table 10. The bridge span is equipped with 2 Bypass Fluid Dampers and both manual and real-time control approaches have been examined to evaluate the response of the bridge structure. For the bare structure increase of the traffic load from H10 to H20S is led to increase the dynamic response of the structure, in terms of displacements in the y-direction from 12.7 to 20.9 mm, 39%, and reaction forces from 1039 kN to 1597 kN, 5.26%, for the speed of 60 miles /hour.

Also, for the same traffic loads (HS20), when the speed of the vehicles increased from 30 m/h to 60 m/h, the loading frequency raised up and resulted more structural displacement in both x and y directions for about 24.4% and the force reaction is increased about 7%. 79.1As it can be concluded from Table 10, for the maximum traffic load and maximum speed, when the valves are closed for 75%, the displacement of the deck of the bridge is reduced about 66.2% in the x-direction and

74.4% in the y-direction. When the valves are fully closed and the device works as a restrainer, displacements in the x-direction, is reduced about 71%, and 79.1% in the y-direction. But the reaction force at the pier of the bridge is increased by 7.8%.

When the real-time control of the bridge-damper model is enabled, the reduction factor of the displacement is regulated based on the fuzzy control algorithm. These values will be changed if the fuzzy rules change. In the assumed control logic, more limitation has been considered for the larger displacements. So, the reduction factor is raised when the load and speed of the vehicles increase. The graphs in Fig. 36 visualize the reduction factor for different loading conditions. In this graph, increases in reaction force at the piers when valves are fully closed are demonstrated. Therefore, the SABFD device, when $\beta = 100\%$, functions as a restrainer and increases the overall stiffness of the structure. So, the importance of real-time control of the structure is highlighted to fulfill the optimum requirements.

10. Conclusion

In this study, a new Integrated Semi-Active Adaptive Vibration Control System (SABFD) comprised a fluid damper with bypass pipe and controllable motorized digital valve, a programmable logic controller (PLC) with an internal fuzzy control algorithm, and displacement sensors are developed and its performance has been assessed numerically and experimentally.

The PLC regulates two motorized electric flow valves to control the flow rate of the oil while moving from one chamber of the hydraulic cylinder to another through bypass pipes according to received data from displacement sensors installed in the bridge deck and pressure transducers installed in the fluid damper. By regulating the flow rate and the pressure inside the fluid damper, the resultant force of SABFD damper and also its function is changing.

The PLC controller performs according to the defined internal fuzzy control rules and therefore, applies a real-time control on the damper device to minimize bridge movement based on the pre-defined program.

To develop the real-time control system, the analytical model of the SABFD device has been developed and then, the fuzzy control algorithm has been defined according to the damper device performance. Afterward, the prototype of the damper device and the PLC controller have been fabricated and several experimental tests include of incremental displacement and cyclic load frequency tests were conducted and the experimental outcomes have been validated through comparison with the results of the analytical model.

The results revealed the following advantageous performance of the device changing of the valve position (β) from 0% (fully open) to 100% (fully close), regulates the performance of the semi-active control system from a passive fluid damper to a restrainer device.

Also, the results proved the effective performance of the PLC controller to adjust the performance of the developed SABFD device according to applied movement using defined fuzzy logic rules.

Thereafter, the application of a developed SABFD system and a real-time control algorithm in a bridge subjected to the traffic load has been made through finite element simulation to assess the effect of a semi-active control system on the response of the bridge.

The outcomes of the study are summarized as follows:

- For the bare structure, increase of the traffic load from H10 to H20S is led to increase of the structure dynamic response in terms of displacements with 39% grow up, and reaction forces with 5.3% increment.
  - For the same traffic loads, when the speed of the vehicles increases from 30 m/h to 60 m/h, displacement is increased about 24.4% and the force reaction is raised up about 7%. Also, the loading frequency raised up and this also resulted more structural displacement and reaction forces at the bridge piers.
  - After implementing the damper devices on the bridge, the values of the displacements are restricted dramatically for all loading conditions.
  - For the fully close status of the valves, the reaction force at the pier of the bridge increased by 7.8%.

Declaration of Competing Interest

The authors declare that they have no known competing financial interests or personal relationships that could have appeared to influence the work reported in this paper.

References

[1] AASHTO Standard Specifications for Highway Bridge. (1996). 16th Edition.
[2] Akcelyan S, Lignos DG, Hikino T. Adaptive numerical method algorithms for nonlinear viscous and bilinear oil damper models subjected to dynamic loading. Soil Dyn. Earthq. Eng. 2018;113:488–502.
[3] Avci A, Karagoz I. A new explicit friction factor formula for laminar, transition and turbulent flows in smooth and rough pipes. Eur. J. Mech. B. Fluids 2019;78:182–7.
[4] Bakhshinezhad S, Mohebbi M. Multi-objective optimal design of semi-active fluid viscous dampers for nonlinear structures using NSGA-II. Structures 2020;24:678–89.
[5] J. Benčat, R. Kohár, (2018). Bridges Subjected to Dynamic Loading. Chapter 7. Intechopen, doi: 10.5772/intechopen.73193.
[6] Bertolesi E, Buitrago M, Adam JM, Calderón PA. Fatigue assessment of steel riveted railway bridges: Full-scale tests and analytical approach. J. Constr. Steel Res. 2021;182:106664.
[7] Escalante-Martınez JE, Gomez-Aguilar JF, Calderon-Ramon C, Morales-Mendoza LJ, Cruz-Ordun I, Laguna-Camacho JR. Experimental evaluation of viscous damping coefficient in the fractional underdamped oscillator. Adv. Mech. Eng. 2016;8(4):1–12.
[8] Heng K, Li R, Li Z, Wu H. Dynamic responses of highway bridge subjected to heavy truck impact. Eng. Struct. 2021;232:111828.
[9] JSSI Manual. (2003). Design and Construction Manual for Passively Controlled Buildings. Japan Society of Seismic Isolation (JSSI), First Edition, Tokyo, JAPAN, in Japanese, 405 pages.
[10] Jugulkar LM, Singh S, Sawant SM. Fluid flow modeling and experimental investigation on automobile damper. Constr. Build. Mater. 2016;121:760–72.
[11] Liu, S. C., Lagorio, H. J., and Chong, K. P. (1991). Status of U.S. research on structural control systems. N/ST Spec. Publ., N-820, U.S. Dept. of Commerce, Nat. Inst. of Standards and TechnoL. Gaithersburg, Md., 211-215.
[12] Losanno D, Londono JM, Zinno S, Serino G. Effective damping and frequencies of viscous damper braced structures considering the supports flexibility. Comput. Struct. 2018;207:121–31.
[13] Maljaars J. Evaluation of traffic load models for fatigue verification of European road bridges. Eng. Struct. 2020;225:111326.
[14] Munson BR, Young DF, Okiishi TH, Huebsch WW. Fundamentals of Fluid Mechanics. sixth ed. John Wiley & Sons Inc; 2009.
[15] Park K-S, Koh H-M, Ok S-Y, Seo C-W. Fuzzy supervisory control of earthquake-excited cable-stayed bridges. Eng. Struct. 2005;27(7):1086–100.
[16] Poplawski B, Mikułowski G, Wiszowaty R, Jankowski Ł. Mitigation of forced vibrations by semi-active control of local transfer of moments. Mech. Syst. Sig. Process. 2021;157:107733.
[17] Soong TT. State of the art review: active structural control in civil engineering. Engrg Struct 1988;10(2):74–84.
[18] Syrakos A, Dimakopoulos Y, Tsamopoulos J. Theoretical study of the flow in a fluid damper containing high viscosity silicone oil: effects of shear-thinning and viscoelasticity. Phys. Fluids 2018;30(3):030708.
[19] Tamai H, Chi L, Yoichi Y. New design concept for bridge restrainers with rubber cushion considering dynamic action: a preliminary study. Appl. Sci. 2020;10(19):6847. https://doi.org/10.3390/app10196847.
[21] Wang L, Nagarajaiah S, Shi W, Zhou Y. Study on adaptive-passive eddy current pendulum tuned mass damper for wind-induced vibration control. Structural Design of Tall and Special Buildings 2020;29(1). https://doi.org/10.1002/tal.1793.
[22] Wang L, Nagarajaiah S, Shi W, Zhou Y. Semi-active control of walking-induced vibrations in bridges using adaptive tuned mass damper considering human-structure-interaction. ISSN 0141-0296 Eng. Struct. 2021;244:112743. https://doi.org/10.1016/j.engstruct.2021.112743.
[23] Wang L, Nagarajaiah S, Shi W, Zhou Y. Seismic performance improvement of base-isolated structures using a semi-active tuned mass damper. ISSN 0141-0296 Eng. Struct. 2022;271:114963. https://doi.org/10.1016/j.engstruct.2022.114963.
[24] Wang L, Shi W, Li X, Zhang Q, Zhou Y. An adaptive-passive retuning device for a pendulum tuned mass damper considering mass uncertainty and optimum frequency. Struct. Control Health Monit. 2019;26(7):e2377.
[25] Wang L, Shi W, Zhang Q, Zhou Y. Study on adaptive-passive multiple tuned mass damper with variable mass for a large-span floor structure. ISSN 0141-0296 Eng. Struct. 2020;209:110010. https://doi.org/10.1016/j.engstruct.2019.110010.
[26] Wang L, Shi W, Zhou Y. Adaptive-passive tuned mass damper for structural aseismic protection including soil–structure interaction. ISSN 0267-7261 Soil Dyn.

Earthquake Eng. 2022;158:107298. https://doi.org/10.1016/j.soildyn.2022.107298.
[27] Wang L, Shi W, Zhou Y, Zhang Q. C) Semi-active eddy current pendulum tuned mass damper with variable frequency and damping. Smart Struct. Syst. 2020;25(1):65–80. https://doi.org/10.12989/SSS.2020.25.1.065.
[28] Wang Y, Wang L, Shi W. Two-dimensional air spring based semi-active TMD for vertical and lateral walking and wind-induced vibration control. Struct. Eng. Mech. 2021;80(4):377–90.
[29] Wasilewski M, Pisarski D. Adaptive semi-active control of a beam structure subjected to a moving load traversing with time-varying velocity. J. Sound Vib. 2020;481:115404.
[30] E.L. Wilson, 1962. Dynamic Response by Step-By-Step Matrix Analysis. Proceedings, Symposium on The Use of Computers in Civil Engineering, Labortorio Nacional de Engenharia Civil, Lisbon, Portugal, 1-5.
[31] Xiang N, Goto Y, Obata M, Alam MS. Passive seismic unseating prevention strategies implemented in highway bridges: a state-of-the-art review. Eng. Struct. 2019;194:77–93.
[32] Xu ZD, Guo YQ, Zhu JT, Xu FH. Intelligent Vibration Control in Civil Engineering Structures. United Kingdom: Elsevier Inc.; 2017. ISBN: 978-0-12-405874-3.
[33] Yu Y, Kurian B, Zhang W, Cai CS, Liu Y. Fatigue damage prognosis of steel bridges under traffic loading using a time-based crack growth method. Eng. Struct. 2021;237:112162.
[34] Zhao D, Li Y. Fuzzy control for seismic protection of semiactive base-isolated structures subjected to near-fault earthquakes. Math. Probl. Eng. 2015;2015:1–17.